Note: This is the author's version of the paper that was published online in Geomorphology on the 7/3/2018 doi: 10.1016/j.geomorph.2018.03.002.

Which DEM is best for analysing fluvial landscape development in mountainous terrains?

Sarah J. Boulton* and Martin Stokes

School of Geography, Earth and Environmental Sciences, University of Plymouth, Plymouth, PL4 8AA, U.K.

**Corresponding author: sarah.boulton@plymouth.ac.uk*

Abstract

Regional studies of fluvial landforms and long-term (Quaternary) landscape development in remote mountain landscapes routinely use satellite-derived DEM data sets. The SRTM and ASTER DEMs are the most commonly utilised because of their longer availability, free cost, and ease of access. However, rapid technological developments mean that newer and higher resolution DEM data sets such as ALOS World 3D (AW3D) and TanDEM-X are being released to the scientific community. Geomorphologists are thus faced with an increasingly problematic challenge of selecting an appropriate DEM for their landscape analyses. Here, we test the application of four medium resolution DEM products (30 m = SRTM, ASTER, AW3D; 12 m = TanDEM-X) for qualitative and quantitative analysis of a fluvial mountain landscape using the Dades River catchment (High Atlas Mountains, Morocco). This landscape comprises significant DEM remote sensing challenges, notably a high mountain relief, steep slopes, and a deeply incised high sinuosity drainage network with narrow canyon / gorge reaches. Our goal was to see which DEM produced the most representative best fit drainage network and meaningful quantification. To achieve this, we used ArcGIS and Stream Profiler platforms to generate catchment hillshade and slope rasters and to extract drainage network, channel long profile and channel slope, and area data. TanDEM-X produces the clearest landscape representation but with channel routing errors in localised high relief areas. Thirty-metre DEMs are smoother and less detailed, but the AW3D shows the closest fit to the real drainage network configuration. The TanDEM-X elevation values are the closest to field-derived GPS measurements. Long profiles exhibit similar shapes but with minor differences in length, elevation, and the degree of noise / smoothing, with AW3D producing the best representation. Slope-area plots display similarly positioned slope-break knickpoints with modest differences in steepness and concavity indices, but again best represented by AW3D. Collectively, our study shows that despite the higher effective resolution of TanDEM-X (12 m), the AW3D (30 m) data performs strongly across all analyses suggesting that it currently offers the greatest potential for regional mountain geomorphological analyses.

Keywords: digital elevation model; digital surface model; river profile; Morocco

1. Introduction

The geomorphological analysis of mountain landscapes has routinely relied on remotely sensed topographic data, traditionally using combinations of aerial/satellite imagery and topographic maps (Bishop and Schroeder, 2004). Over the years, the remote sensing of such regions has been revolutionised by an exponential increase in the availability of easily accessible, high quality, and low cost digital elevation models (DEMs) (Moore et al., 1991). These digital topographic data sets have allowed for rapid and easy extraction of geomorphic parameters and their quantification for a wide range of mapping and visualisation purposes (e.g., Schneevoigt et al., 2008; Smith and Pain, 2009), with even minimal GIS expertise. In particular, the quantitative study of bedrock fluvial geomorphology in upland areas has been a focus of many studies, commonly utilising global data sets such as those produced by the Shuttle Radar Topography Mission (SRTM) and the Advanced Spaceborne Thermal Emission and Reflection Radiometer (ASTER) to undertake regional analyses (i.e., Wobus et al., 2006; Boulton and Whittaker, 2009; Kirby and Whipple, 2012; Whittaker and Boulton, 2012; Fisher et al., 2013; Antón et al., 2014; Kent et al., 2017; Rossi et al., 2017; Sinclair et el., 2017; Stübner et al., 2017).

The advent of very high resolution LiDAR (Light Detection And Ranging) data and a resurgence in Structure from Motion (SfM) analyses (Westoby et al., 2012), owing to the production of low cost aerial drones, has allowed the investigation of previously unresolvable geomorphic landforms (e.g., DiBiase et al., 2012; Fonstad et al., 2013; Roering et al., 2013; Micheletti et al., 2015). However, the restricted spatial coverage of such data sets cannot compete with the medium resolution satellite-derived DEMs. Furthermore, LiDAR and SfM data collection typically have individually financially costly hardware requirements, as well as the need for onsite fieldwork to collect the data. Therefore, local data sets are unlikely to supersede global models in the near future. In addition to near global data coverage, the strengths of satellite-derived data sets also lie in the fact that many are made freely available to all, or at low cost to the scientific community, and have undergone exacting data validation and extensive ground correlation (e.g. Hirano et al., 2003; Mukherjee et al., 2013). The DEMs also facilitate topographic analyses in remote areas that would otherwise be topographically or politically difficult to access. However, the accuracy of the results is dependent on the quality and parameters of the DEM, such as the resolution and the presence of errors or voids in the data. High relief, mountainous regions that are of particular interest to fluvial and tectonic geomorphologists are especially prone to DEM errors owing to topographic shadowing and layover phenomena (Toutin, 2002).

With the recent release of the final 12 m TanDEM-X DEM product by the German Aerospace Centre (DLR, 2016) and the void-filled 30 m ALOS World 3D (AW3D30) DEM by the Japanese Aerospace Exploration Agency (JAXA), more global DEMs are available to choose from than ever before when undertaking geomorphic analyses. Both of these new products aim to improve accuracy, especially in areas of high mountain relief. However, how do these new data sets compare against the existing SRTM or ASTER data, and collectively, which DEM data set offers the best opportunity for visualisation and quantitative analysis of fluvial geomorphological features within mountain landscapes?

To contribute to this topic we will investigate how the new TanDEM-X DEM (TanDEM-X hereafter) and AW3D30 DEM compare to the established 1” (30 m) SRTM DEM (referred to as SRTM30) and the ASTER GDEM v2 (referred to as ASTER) for

standard fluvial geomorphic analyses in a mountain landscape undertaken in ArcGIS 10.3 and Matlab. We have selected the High Atlas Mountains in northwest Africa and specifically the Dades River catchment to undertake the comparative DEM analyses. The High Atlas Mountains reach peak elevations of 3500 to 4000 m, with an average elevation of 2000 m and frequent high local reliefs of >1000 m. The location of the High Atlas on the margins of the Sahara Desert results in a low vegetation cover providing landscape clarity, and a low population density with little human impact on shaping the landscape, indicating that fluvial geomorphic processes are natural. The remote nature of the mountains means that field access to the landscape can be challenging, and thus, remote sensing through DEM analysis is an ideal analytical approach.

Furthermore, we have published field and remote sensing experiences on many aspects of its fluvial geomorphology and its role in broader mountain landscape development contexts (Stokes et al., 2008, 2017; Boulton et al., 2014; Stokes and Mather, 2015; Mather and Stokes, 2017; Mather et al., 2017). More specifically, the late Cenozoic fluvial landscape development has resulted in a deeply incised drainage network with narrow and high sinuosity valleys that show varied concordance / discordance with the underlying Mesozoic bedrock geology, with a notable active and passive tectonic control on the drainage pattern, routing, and evolution (e.g., Stokes et al., 2017). Thus, the broader region and specifically the Dades River catchment is an ideal test site for assessing the usefulness and accuracy of the different DEMs. We achieve this by undertaking a qualitative and quantitative assessment of the DEM data sets, highlighting the pros and cons for visualising key aspects of the fluvial landscape and for the extraction and analysis of river long profiles.

2. Data sets

2.1. SRTM DEM

In 2000, NASA launched its Shuttle Radar Topography Mission (SRTM) on the space shuttle Endeavour. Most of the Earth's surface (99.97%) between 60°N and 56°S was scanned over 11 days using a synthetic aperture radar (SAR) interferometer, comprising two radar antennas 60 m apart (e.g., Werner, 2001; Rodriguez et al., 2005). The DEM generation was achieved with at least two interferometric pairs with opposing viewing perspectives (Rabus et al., 2003; Smith and Sandwell, 2003) using a C-band radar system for the main data collection (Farr et al., 2007). Radars were unable to penetrate dense vegetation canopies, meaning that the DEM generally represents a canopy top model (Farr et al., 2007).

Until September 2014, SRTM data were provided at 3 arc second (~90 m) spatial resolution for most of the world apart from the USA where 1 arc second (~30 m) data were available. Subsequently, the 1 arc second data was released globally and is available through the USGS EarthExplorer interface (https://earthexplorer.usgs.gov/). The absolute vertical accuracy of the DEM is better than 9 m (Rodriguez et al., 2005, 2006) using the EGM96 vertical reference frame. However, although void-filling of the SRTM data has been undertaken (e.g., Jarvis et al., 2008) the current 1 arc second SRTM30 release still possesses voids in the data set. Despite this, SRTM data is one of the most utilised DEMs being cost free and easily accessible.

2.2. TanDEM-X DEM

The TanDEM-X mission is based on the utilization of the two X-band radar satellites TerraSAR-X and TanDEM-X flying in formation with an adjustable baseline of between 100 and 500 m. Thus, a flexible single-pass SAR interferometer is able to generate a high resolution and consistent DEM for all landmasses including Antarctica but excluding latitudes above 60°N (DLR, 2016). Data acquisition took four years from December 2010 to January 2015 covering all landmasses at least twice. Because elevations are defined with respect to the reflective surface of the X-band SAR returns, the product is predominantly a surface model like the SRTM DEM (DLR, 2016).

The global TanDEM-X DEM was released to the scientific community in December 2016 for the two highest posting classes of 12 and 30 m. Absolute vertical and horizontal accuracies of the 0.4 (~12 m) arc second product TanDEM-X DEM are stated as <10 m with the vertical datum of WGS84-G1150 used (DLR, 2016). Note that this product is not referenced to the EGM96 vertical reference frame. In addition to the DEM, a number of information layers (i.e., height error map, consistency mask, etc.) are provided with the data to facilitate quality assessment of the resultant DEM.

2.3. ASTER GDEM

The Advanced Spaceborne Thermal Emission and Reflection Radiometer (ASTER) is a sensor on the TERRA satellite, a joint mission between NASA and the Japanese Ministry of Economy, Trade and Industry (NASA, 2001). The first data release in June 2009 (GDEM1), used >1.2 million near-infrared stereo-pair images to generate a global DEM spanning from 83°N to 83°S at a 1 arc-second grid spacing, although data issues resulted in an effective spatial resolution of ~120 m (Tachikawa et al., 2011). The second version was released in 2011, with improved coverage and reduced artefacts owing to the incorporation of 260,000 additional stereo-pairs increasing the horizontal and the vertical accuracy of the product (Tachikawa et al., 2011). The effective resolution of the GDEM2 is estimated to be 70-82 m, resulting in a 35% improvement over the GDEM1 and similar to the STRM30 resolution. The GDEM2 also uses the EGM96 vertical reference frame (Tachikawa et al., 2011). The ASTER DEM is available through the NASA EarthData portal (https://search.earthdata.nasa.gov/search).

2.4. AW3D30 DEM

The Japan Aerospace Exploration Agency (JAXA) released a global DEM with a horizontal resolution of ~30 m in May 2016 and an updated void-filled product in March 2017 (available from http://www.eorc.jaxa.jp/ALOS/en/aw3d30/index.htm). The data set was compiled from images acquired by the Panchromatic Remote-sensing Instrument for Stereo Mapping (PRISM) on board the Advanced Land Observing Satellite (ALOS) between 2006 and 2011. The full DEM spans regions up 82°N and S, but the void-filled DEM is restricted to 60° N/S owing to issues with cloud and snow cover. Around 3 million scenes with <30% cloud cover were used to generate a 0.15-arcsec DEM (Tadono et al., 2014), which was resampled to produce the global 30-m DEM available in two formats, ‘average’ and ‘median’, with a height accuracy of <5 m (Tadono et al., 2016) using the EGM96 vertical reference frame. The ‘average’ DEM

was produced by averaging 49 pixels (7 x 7) to obtain the final pixel value. Whereas the 'median' method selected the median height value, i.e., the 25th height from 49 pixels to derive the final pixel value (Tadono et al., 2016). In this study, the 'average' DEM is used.

2.5. Previous work

Numerous studies have compared the 30-m ASTER data set to either the 90- or 30-m SRTM DEM for a range of geomorphic applications (i.e., Hirt et al., 2010; Frey and Paul, 2012; Suwandana et al., 2012; Wang et al., 2012; Fisher et al., 2013; Das et al., 2016). Generally, ASTER data possesses a lower effective resolution and is less accurate than the SRTM data for geomorphic applications in line with the published validation data (NASA, 2001; Tachikawa et al., 2011).

Fewer studies have considered the newer DEM data sets. Purinton and Bookhagen (2017) compared geomorphic metrics derived from four DEMs of different spatial resolution (30-m SRTM, 12-m TanDEM-X, 10-m CoSSC TDX, and 5-m ALOS World 3D (AW3D5) [the higher resolution version of the AW3D30 data]) using the Central Andean Plateau. They investigated the variability of several fluvial geomorphic indices finding consistent values across different data sets. They also discovered that the AW3D5 data was very noisy, especially compared to the TanDEM-X DEM. However, in their study only the SRTM data is publically available with the other data sets either commercially acquired (AW3D5) or post-processed by the authors prior to the widespread release of the final data products (TanDEM-X and CoSSC radar pairs). The analyses of Purinton and Bookhagen (2017) required a significantly high degree of GIS expertise to undertake the required processing.

Hu et al. (2017) compared 30-m SRTM and ASTER data with the newer, and publicly available, 30-m AW3D30 data set to investigate accuracy with respect to landcover and relief for selected study areas in the mountainous Hubei province of China. As with previous studies, they found the ASTER GDEM to be less accurate than the other DEMs, with the SRTM and AW3D30 data having practically the same quality. However, Hu et al. (2017) noted that the SRTM DEM provides slightly better accuracy in mountainous high relief areas.

The relative ease of extracting fluvial geomorphic information from DEMs has also led to a proliferation of river long profile studies in recent years (e.g. Chen et al., 2003; Kirby, 2003; Whittaker et al., 2007; Boulton and Whittaker, 2009; Yanites and Tucker, 2010; Kirby and Whipple, 2012; Regalla et al., 2013; Boulton et al., 2014; Kent et al., 2017; Martins et al., 2017; Petit et al., 2017; Roda-Boluda and Whittaker, 2018). Whilst the accuracy of channel network extraction has been investigated for a range of geomorphic terranes and data resolutions (e.g., Tarboton et al., 1991; Walker and Willgoose, 1999; McMaster, 2002; Ariza-Villaverde et al., 2015; Persendt and Gomez, 2016; Schneider et al., 2017), few authors have investigated the effect of different DEM data sets on fluvial long profile extraction. This is despite known differences in channel slopes being recorded between field surveys and remotely sensed DEMs (e.g., Montgomery et al., 1998; Massong and Montgomery, 2000), as well as the recognition that derived slope is sensitive to DEM grid size (Zhang and Montgomery, 1994; Walker and Willgoose, 1999; Zhang et al., 1999; Finlayson and Montgomery, 2003). Wobus et al. (2006) compared river long profiles and slope data for 30- and 90-m SRTM and for 10- and 30-m USGS DEMs of the San Gabriel Mountains (southern California), finding that extracted topographic indices (concavity and

steepness indices) were consistent within 10% regardless of the data set or choice of smoothing window size. By contrast, the slope-area analysis undertaken by Hancock et al. (2006) for Australian rivers showed marked differences in steepness index between 90-m SRTM data and a 20-m DEM developed from photogrammetry.

Collectively, more research is clearly needed to understand the fluvial geomorphic limitations of commonly used topographic data sets and to assess the potential of the new global data sets in comparison. This will allow the geomorphic community to make more informed decisions about which data set to use for topographic analyses in mountain landscapes.

3. Principles of river profile analysis

Topography has long been recognised to record the interplay between tectonic rock uplift, climate, and lithology with rivers carving relief and dictating the pace at which the landscape responds to base-level change (Gilbert, 1877; Davis, 1903; Kirby and Whipple, 2012). The DEMs have greatly facilitated the analysis of mountain river systems and determined the empirical evidence for the use of river long profiles in tectonic studies (i.e., Chen et al., 2003; Kirby, 2003; Whittaker et al., 2007; Boulton and Whittaker, 2009; Yanites and Tucker, 2010; Kirby and Whipple, 2012; Regalla et al., 2013; Boulton et al., 2014; Kent et al., 2017; Roda-Boluda and Whittaker, 2018). Key to this approach is the assumption that upland bedrock rivers behave as detachment-limited systems, where the steady-state (erosion equals uplift) river gradient is controlled by the erodibility of the channel substrate and the regional uplift rate or base-level fall (see Kirby and Whipple, 2012, for a complete review). Models of river behaviour predict a power law relationship between local channel slope S and upstream drainage area A:

$$S = k_s A^{-\Theta} \quad (1)$$

Parameters S and A can be extracted from DEMs and slope-area plots generated using GIS software. Subsequently, the concavity index Θ and the steepness index k_s can be derived from the regression of slope and area data on a log-log graph.

The S-A relationship describes why steady-state river long profiles have concave-up shapes (Whipple and Tucker, 2002; Kirby, 2003) and variations in steepness index have been linked to different uplift rates (Synder et al., 2003; Wobus et al., 2006). However, not all river long profiles exhibit a graded concave-up profile, and many have discontinuities in their long profiles where local channel slope dramatically increases; these features are termed knickpoints or knickzones (e.g., Kirby and Whipple, 2012). Knickpoint presence is often indicative of a river undergoing a transient response to a persistent change in relative base level, such as a change in rock uplift rate. A discrete event (such as a locally resistant substrate, a debris flow or landslide) will generate a 'vertical-step knickpoint' (Haviv et al., 2010; Kirby and Whipple, 2012; Walsh et al., 2012) that can be recognised on a slope-area plot as a spike in slope values. Vertical-step knickpoints are normally anchored in space and likely have no direct tectonic significance (Kirby and Whipple, 2012). By contrast, 'slope-break knickpoints' (Haviv et al., 2010; Kirby and Whipple, 2012) represent a discontinuity in slope-area scaling, recognised by an increase in the steepness index, that develops in response to a tectonic forcing that causes a perturbation in the fluvial system (Tucker and Whipple, 2002); e.g., owing to the initiation of faulting or to an increase in slip rate along a fault. Therefore, slope-break knickpoints can facilitate the recognition of active tectonics in erosional landscapes (Wobus et al., 2006; Kirby and Whipple, 2012).

4. Study area

The Dades River is a major perennial river and the principal drainage system in the south-central High Atlas Mountains, with a catchment area of >1600 km^2. The headwaters rise at ~3200 m with the river flowing SW through the fold-thrust belt region of the core of the mountain belt in a series of bedrock meanders and deeply incised gorges. It passes through the Ait Sedratt thrust top basin and the main South Atlas thrust front region before entering the Ouarzazate foreland basin (Fig. 1) where it becomes the major regional trunk drainage. The river is routed along the southern margin of the Ouarzazate Basin and northern mountain front of the Anti-Atlas (Stokes et al., 2008; Babault et al., 2012). At Ouarzazate town, the Dades River turns to the SE to become the Draa River, crossing pre-Cambrian and Palaeozoic bedrock of the Anti-Atlas Mountains through the Draa Gorge to eventually flow into the Atlantic Ocean.

The Quaternary development of the Dades River and its tributaries is recorded by a series of inset river terraces and stepped alluvial fan and pediment surfaces (Stablein, 1988; Arboleya et al. 2008; Pastor et al., 2012; Stokes et al., 2017). In areas of structurally thickened limestone, the Dades River has formed deeply dissected river gorges such as the Dades and Tarhía n'Dades gorges (Stokes et al., 2008; Boulton et al., 2014). The overall incisional pattern of the drainage network, including river gorge development, is considered to primarily reflect the long term tectonic uplift of the High Atlas orogenic system (Stablein, 1988; Stokes et al, 2008, 2017; Babault et al., 2012). Boulton et al. (2014) showed that the river long profile of the Dades River contained knickpoints, marking the upstream extent of areas of incision and gorge formation. These and similar knickpoints in adjacent rivers were interpreted to have formed from a transient response to tectonic rock uplift (Boulton et al., 2014). Boulton et al. (2014) used the 90-m SRTM data for their analysis as the 30-m ASTER data was found to be of lower quality, but this resulted in the gorge regions, higher sinuosity valleys, and canyon reaches being poorly resolved.

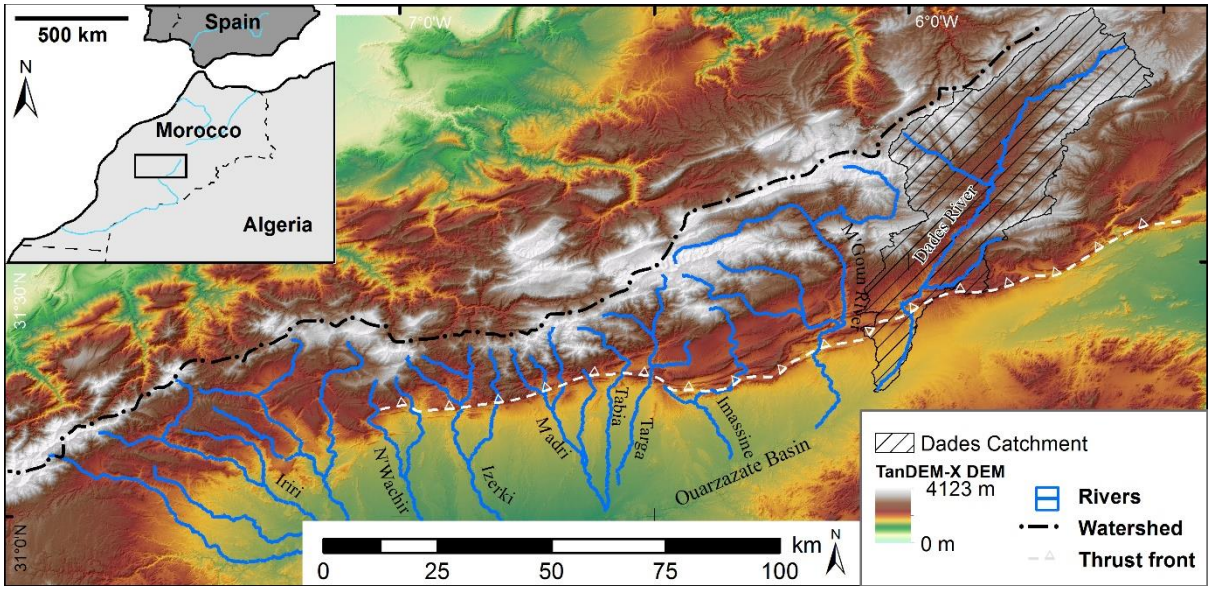

Fig. 1. TanDEM-X data (© DLR 2017) showing a regional overview of the Central High Atlas Region (Morocco) and the location of the Dades River catchment, modified from Boulton et al. (2014). FTB = Fold Thrust Belt; WTB = Wedge top basin (Ait Sedratt); TF = Thrust Front (Southern Atlas); FB = Foredeep basin. Inset map showing location of the study area in NE Africa.

Superimposed onto the high relief caused by this tectonic uplift are sedimentation and erosion patterns, such as river terrace sequences, linked to Quaternary climatic fluctuations and the underlying strength of the bedrock lithology (Stokes et al., 2017). At the present time the area is characterised by a semiarid climate with altitudinal zonation, where annual precipitation varies from ~150 mm/a in the basin to 200 mm/a in the headwaters (Schulz et al., 2008; Dłużewski et al., 2013).

5. Methods

All four data sets used in this study were analysed within ArcGIS 10.3 and Matlab R2016a. The aim was not to undertake complex statistical analyses of these data (c.f., Pipaud et al., 2015), but rather investigate the difference in the results of common fluvial geomorphic analyses undertaken on each DEM.

The study area covers multiple tiles for the different DEMs, and for all of the data sets three tiles were used in this study (N31_W007; N31_W006, N32_W006) all provided with geodetic reference of WGS84. Prior to further analysis, the tiles were mosaicked and projected to UTM Zone 29N using bilinear interpolation. Using a projected coordinate system allows the common derivatives of hillshade and slope to be generated and used to evaluate the level of landscape detail visible in each of the DEMs.

In addition, the TanDEM-X data is supplied with heights given with respect to a reference ellipsoid (the ellipsoid height), whereas the other three DEMs are supplied with heights given above the geoid (the orthometric height). Therefore, the TanDEM-X heights need to be converted to orthometric heights otherwise a vertical offset is introduced between the different data sets. For Morocco, this difference is ~50 m. This transformation was undertaken in ArcCatalog using the mosaic data set feature type in a geodatabase.

Subsequently, the drainage network and catchment area for the Dades River was extracted using the widely adopted Arc hydrology tools (e.g., Fill, Flow Direction, Flow Accumulation). A condition evaluation used 10,000 pixels as the threshold value for the stream network generation for the SRTM30, ASTER GDEM2, and AW3D30 data sets and a higher threshold of 100,000 pixels was used for the TanDEM-X data to compensate for the smaller pixel size and thus greater number of pixels contributing to the flow accumulation raster. The different networks generated through the D8 algorithm (O'Callaghan and Mark, 1984) employed by ArcGIS were then compared to the river on satellite imagery from Google Earth.

Using the Geomorphtools 'stream profiler' (http://geomorphtools.geology.isu.edu/), the long profile of the Dades River, the channel slope S and drainage area A as a function of downstream distance L was derived from each DEM (Eq. 1). This plugin allows the channel steepness index k_s and the concavity θ to be calculated for each reach of the Dades River (Eq. 1). A reference concavity θ_{ref} of 0.45 was used to derive k_{sn}, the normalised steepness index (c.f. Wobus et al., 2006), to enable comparison between each dataset. As several knickpoints are present in the long profile (Boulton et al., 2014), normalised steepness indices were derived for each channel reach that can be commonly identified across each data set.

Finally, in order to evaluate the DEM accuracy against field data, we plot elevation data measured in the field using handheld GPS, either a Garmin GPS60C or a Trimble GeoXH. Real-time-post-processing using ground station corrections resulted in vertical accuracies of <3 m against the pixel value at that location for 77 field locations spanning four field visits undertaken in May 2011 to May 2014.

Additional quality control using auxiliary data sets is possible for the ASTER, AW3D30, and TanDEM-X data (supplemental data). Here, the overall quality of the data is important to investigate as voids or other data processing issues can seriously affect the usability of the data. For SAR data in particular, the interferomic coherence is the primary quality measure, while decorrelation can cause random noise and roughness in the DEM (Geudtner, 1995). Furthermore, void recognition and the number of image pairs used in the processing have implications for the overall DEM quality. Whilst the number of images used (stacked) to create the DEM is also an important quality indicator for the ASTER and AW3D30 data sets.

6. Results

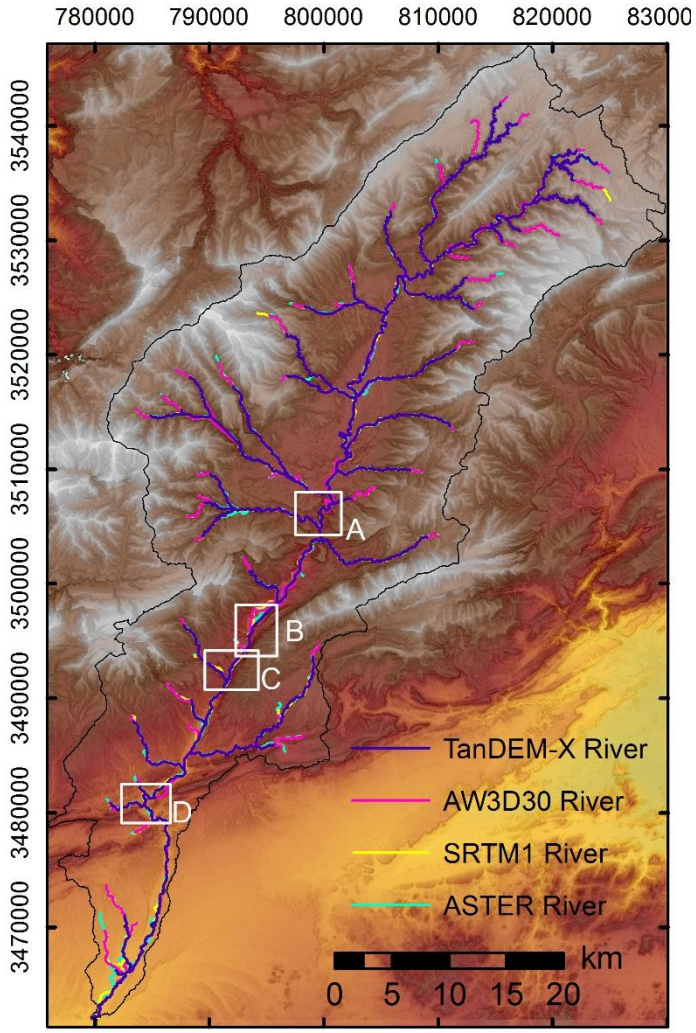

To assess and compare the differences between the four DEMs, we examined the Dades catchment within the High Atlas (encompassing the foreland basin margin, thrust front, wedge top basin, and fold-thrust belt regions). Within this catchment we targeted four key areas that have been visited in the field and represent challenging areas for satellite-derived data comprising steep and highly incised terrain, including high sinuosity canyons / bedrock meander systems (Fig. 2; areas A and B) and narrow gorges (Fig. 2; areas C and D)

Fig. 2. TanDEM-X DEM (© DLR 2017) for the Dades catchment showing the catchment area and the river networks generated using the ArcHydrology tool box for the four DEMs investigated. Boxes indicate position of detailed subareas (Figs. 4, 8, 9, 11).

There are visual and quantitative differences between the TanDEM-X, SRTM30, AW3D30, and ASTER GDEM2 DEMs for the Dades River catchment. The TanDEM-X offers the clearest visualisation for the hillshade and slope rasters of area, with scarps, ridges, and fluvial channels being rendered in great detail. However, in areas

of high relief, such as the inner channel of many streams or along escarpments, the raster loses sharpness, and topographic detail is lost owing to significant areas of roughness with high slope values (i.e., Fig. 3). These locations are clearly visible as areas on the quality control rasters as regions with height errors of up to 4–5 m, as a result of at least one inconsistent height pair (7.7% of all pixels), shadows or layovers (0.03%), or for 0.5% pixels the erroneous detection of waterbodies at the 1–3 times coherence threshold (Appendix Fig. A). Notably, the number of valid height values from different DEM acquisitions is variable, generally with 5 to 8 coverages in different parts of the study area but some of the problem areas have fewer.

By contrast, the three 30-m DEMs are smoother and contain less detail, although in most cases the shape and position of the main river channel is well defined in all data sets. Although the posting of the DEMs is the same, clear differences are apparent between the AW3D30, SRTM30, and ASTER DEMs. Interestingly, the effective resolution of the SRTM30 and ASTER GDEM2 data sets should be comparable (ASTER DEM Validation Team, 2011), but an inspection of the ASTER data for the Dades reveals that the main tile (ASTGTM2_N31W006) covering the area has not been improved over the earlier GDEM1 product, yet the adjacent tiles have been upgraded. The effect of the differing effective resolution can be seen in the far north and west of the area where parts of the adjacent tiles form the catchment area (i.e., Fig. 2; area D).

By contrast, the new AW3D30 DEM is sharper and more detailed than either the SRTM30 or ASTER products. Topographic detail is clearly rendered even in areas of high relief and steep topography unlike the TanDEM-X. The quality assurance data indicates that >99% of the catchment contains valid heights with only a few pixels affected by low correlation as a result of the inferred presence of inland water (Appendix Fig. B).

The SRTM30 DEM offers the third best representation of the landscape after the TanDEM-X and AW3D30 DEMs. The landscape is smoothed but also does not suffer the roughness in high relief areas that can be observed on the TanDEM-X data. Whilst small data voids are absent for the Dades catchment the very northernmost tip of the catchment area is missing 1.7 km^2 owing to a mismatch or missing sliver between the adjacent tiles (Appendix Fig. B). Given the small area that this issue effects, this region has been omitted from further analysis, but this issue could have been a significant problem if it had occurred elsewhere in the study area.

The ASTER data is characterised by an even smoother and lower resolution product, despite having the same grid size as the SRTM30 and AW3D30 data. Where the data have been improved, the resulting DEM is similar in resolution to the SRTM30 DEM. However, unlike the other DEMs, the ASTER DEM has a number of small negative elevation anomalies known as pits, some of which are >100 m deep. These pits are clearly related to the stack number patterns, and presence of filled voids is shown in the quality assessment data (Appendix Fig. C). However, <0.01% of total pixels are voids that have been filled by SRTM90 data. Furthermore, the number of image pairs used to create the DEM is variable across the area ranging from 1 to 23 image pairs, with a mean of 15 (Appendix Fig. C). Only 4.9% of the study area was processed from 10 or fewer stereopairs, recognised as a threshold for the quality of topographic representation in ASTER data (Tachikawa et al., 2011).

6.1. Individual areas - results of flow algorithm

Area A (Fig. 4) was selected for study as it represents the upstream extent of the main Dades River knickpoint (Boulton et al., 2014). As a result of the progressive uplift-driven incision of the Dades River, bedrock meanders of ~200 m deep have been carved into the Jurassic marine limestones (Figs. 5A-C). Small river terrace fragments below the resolution of all products have been documented at 140 m above present river level (Stokes et al., 2017) and a large landslide complex is associated with the high relief landscape (Fig. 6).

All three DEMs show the incised nature of the landscape, but the TanDEM-X data is by far the most detailed, with crisp rendering of small channels and even some hummocky detail in the landslide complex (Figs. 4 to 7). However, the AW3D30 nearly matches the visualisation quality of the TanDEM-X data. The TanDEM-X data does suffer from significant roughness in the slopes adjacent from the main channel margins unlike the other DEMs. This is reflected by higher average slope angle of the TanDEM-X data (Table 1) compared to the other data sets.

When the stream networks generated with the Arc hydrology tool box are compared greater differences between the results are observed (Fig. 7). The ASTER network is the least complex and has smoothed out many of the meanders in the river often cutting across the meander necks. In contrast, the AW3D30, SRTM30, and TanDEM-X derived networks are more complex and follow the real course of the river to a greater extent. The main test is in the northern bedrock meander (Figs. 5B and C), here only the SRTM30 and AW3D30 derived networks route correctly around the meander bend, unlike the stream network derived from the TanDEM-X or ASTER DEMs.

Table 1 Minimum and maximum elevations and mean slope angles (values in brackets indicate standard deviation) calculated from the TanDEM-X, SRTM30, ASTER GDEM2, and AW3D30 DEMs for the whole Dades River catchment and areas A–D (Fig. 2)

	Minimum elevation				Maximum elevation				Mean elope			
	TanDEM	SRTM	ASTER	AW3D30	TanDEM	SRTM	ASTER	AW3D30	TanDEM-X	SRTM	ASTER	AW3D30
Whole Catchment	1492	1437	1434	1444	3495	3439	3457	3438	19.13 (10.61)	16.38 (10.02)	15.97 (9.89)	18.12 (10.58)
Area A	1825	1842	1833	1837	2496	2489	2474	2499	22.9 (12.02)	20.18 (11.19)	18.46 (9.81)	21.44 (11.30)
Area B	1701	1708	1710	1701	2723	2691	2716	2734	23.78 (11.15)	20.77 (10.69)	19.30 (10.19)	22.12 (10.61)
Area C	1632	1654	1654	1654	2686	2650	2657	2693	22.60 (9.89)	18.52 (9.78)	18.72 (9.66)	20.98 (9.44)
Area D	1555	1556	1536	1559	2070	2025	2094	2071	19.75 (10.66)	14.25 (9.93)	15.67 (9.32)	17.13 (9.96)

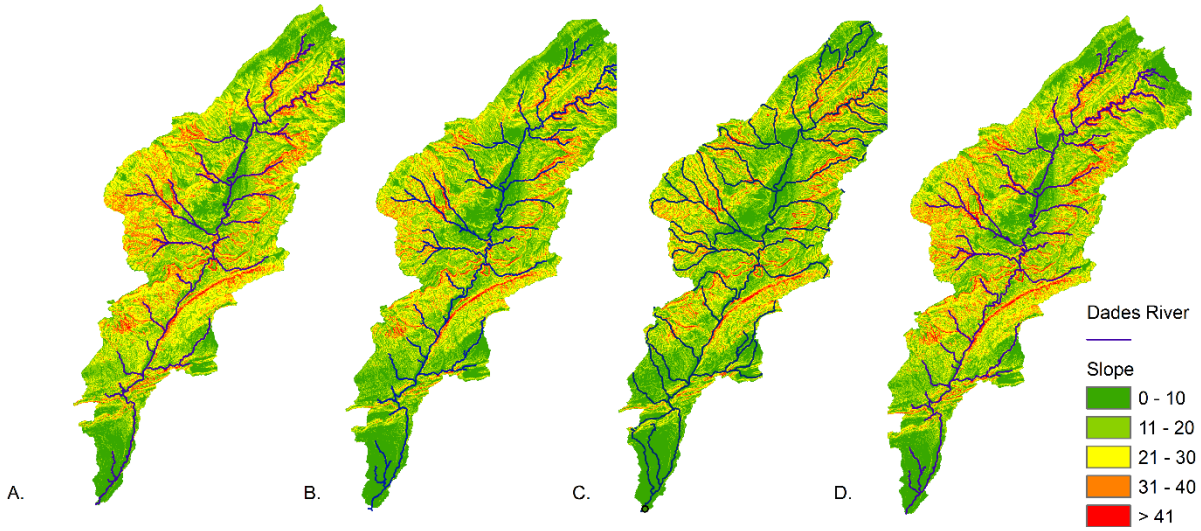

Fig. 3. Slope area map of the Dades catchment for (A) TanDEM-X; (B) SRTM30; (C) ASTER, and (D) AW3D30 DEMs.

Area B (Figs. 7B and 8) is a reach of sinuous and slightly entrenched meanders in an open valley (Fig. 5E) where the river is routed to the SW along the axis of an open syncline fold structure (Stokes et al., 2017). In this region up to three river terrace levels at 10, 20, and 30 m above the modern river channel record a long-term incision trend. To the SE of the present valley is a 350-m-high scarp that separates the modern river valley from the perched Imdîazène palaeovalley, a former river route prior to the creation of the Tarhia n'Dades gorge (Figs. 5D and 7B) (Stokes et al., 2008).

While the effective resolution of the ASTER DEM is the lowest of the DEMs, the resulting slope raster characterises the main river channel to a greater degree than the SRTM data, which depicts the channel and surrounding floodplain as essentially flat. Neither of these DEMs shows much detail of the palaeovalley and both appear to contain small pits. By contrast, the TanDEM-X and the AW3D30 DEMs reveal a high level of geomorphic detail including a cut off bedrock meander reach (Stokes et al., 2017) and detail of bedrock bedding orientations. Although the TanDEM-X data is the most detailed, it is remarkable that the 30-m AW3D30 DEM shows so many small-scale features. The TanDEM-X DEM also has the highest average slope (Table 1).

Interestingly, none of the stream networks generated from the DEMs honours the actual course of the river particularly well (Fig. 7B). Stream networks are oversimplified and contain long straight sections, despite the level of detail seen on the DEM. However, the AW3D30 data has generated a stream network that is fairly representative in the upper section of the meanders but less clear in the downstream section, again straightening out a number of the meander bends across their necks.

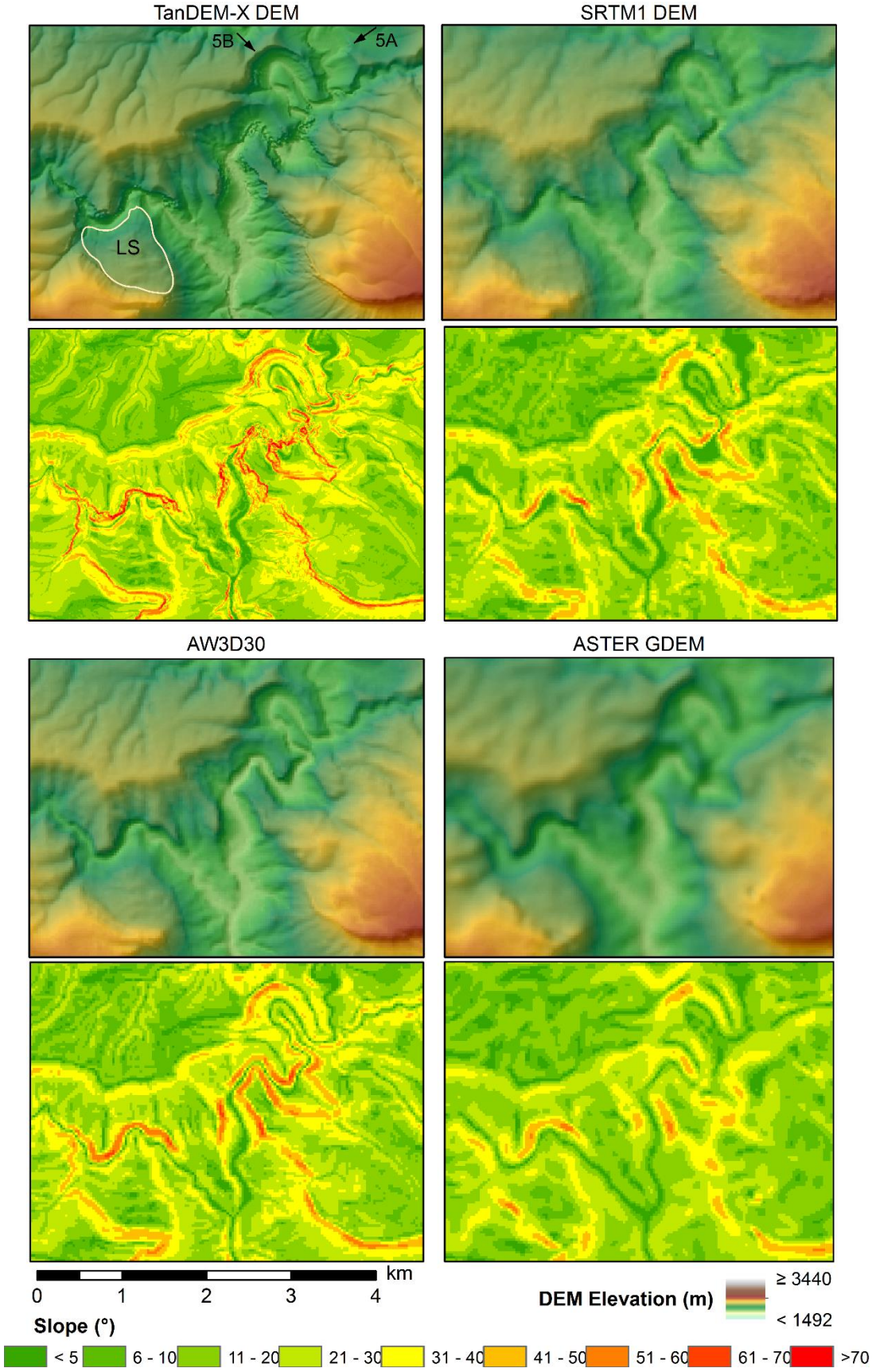

Fig. 4. DEM with underlying hillshade and slope raster for subarea A showing the difference between the four DEMs studied. The location and direction of photographs 5A and 5B are indicated, along with the location of the landslide shown in Fig. 6.

Fig. 5. (A) Looking upstream near the top of the bedrock meanders and the top of the lower Dades River knickzone (Fig. 4). (B) Major bedrock meander incised into Jurassic limestone, this feature is only shown in the stream networks generated from the SRTM30 and AW3D30 data (Fig. 4). (C) View of same meander highlighting the narrow neck of the meander. These meanders are clearly seen in the DEMs in Fig. 3. (D) View to the NE along the Imdîazène palaeovalley (Fig. 8). (E) Looking down onto the village of Imdîazène and the incised meandering river poorly represented by the DEM-derived stream networks (Fig. 8). (F) Looking downstream toward the start of the Tarhía n'Dades Gorge (Fig. 8). (G) Looking downstream to the start of the main Dades Gorge showing structural thickening of Jurassic bedrock and the slot canyon nature of the gorge (Fig. 9). (H) Looking toward the start of the canyon in the fold and thrust belt, which is only clearly seen on the AW3D30 DEM (Fig. 11).

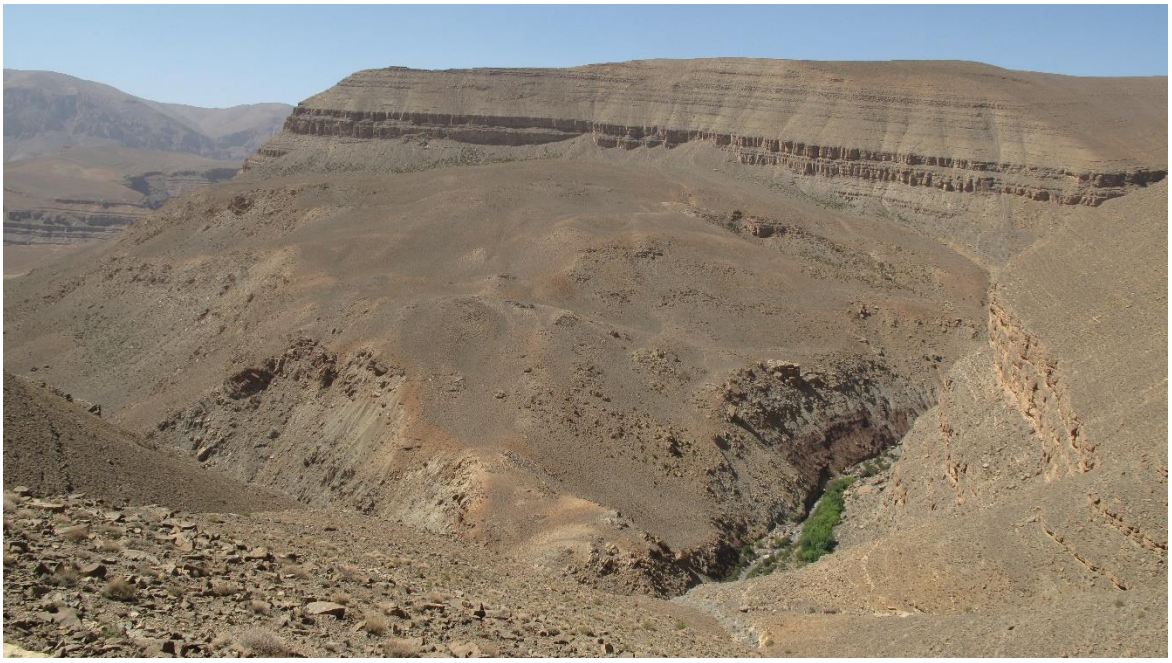

Fig. 6. Photograph (view to the southwest) showing a large landslide located in the Dades River catchment (location, LS, shown on Fig. 7A) located in area A (Fig. 4).

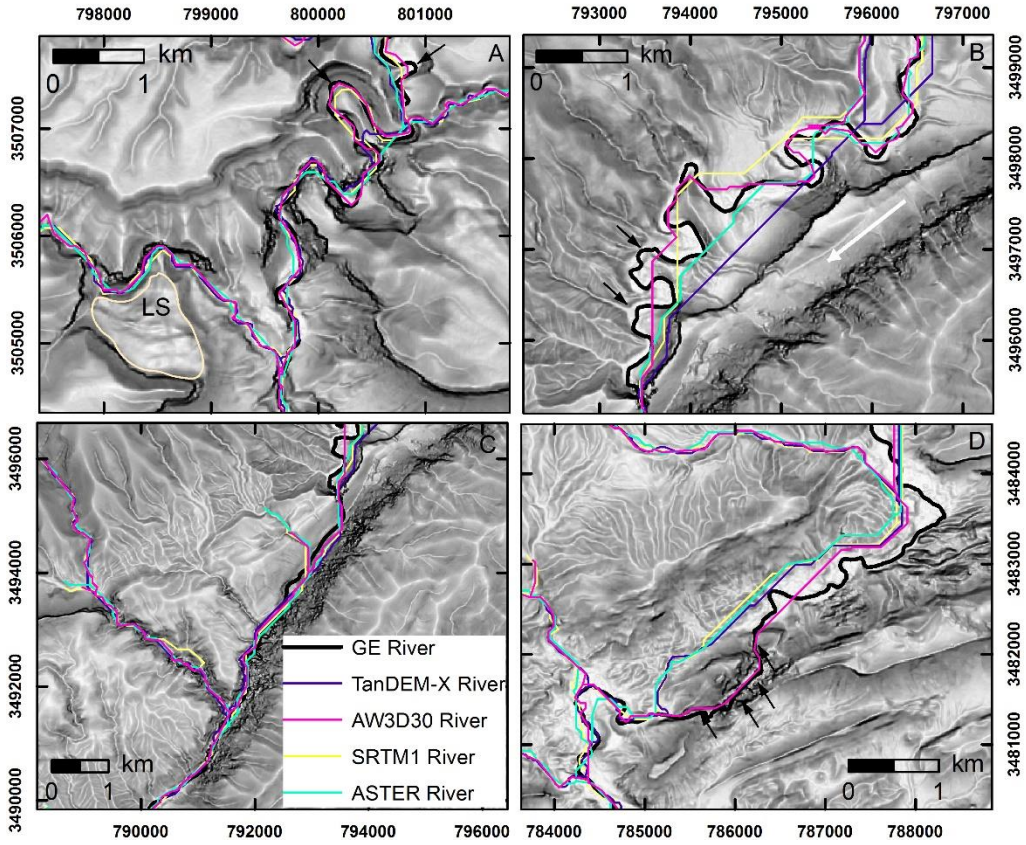

Fig. 7. Greyscale slope rasters extracted from the TanDEM-X DEM (© DLR 2017) for subareas A–D with derived stream networks from all three DEMs and traced from satellite imagery in Google Earth (GE - black line). Black arrows indicate areas where the extracted river network poorly models the river system as traced from Google Earth. On (A) the outlined yellow area (labelled LS) indicates the extent of a large landslide (Fig. 5), and on (B) the white arrow indicates the location and flow direction of the Imdîazène palaeovalley.

Area C is larger than areas A or B at 58 km^2 to encompass the main Dades Gorge and the smaller upstream Tarhía n'Dades Gorge to the north, as a result there is a small overlap with the southern extent of area B (Fig. 9). The Tarhía n'Dades Gorge (Fig. 10A) is a NW-SE orientated narrow (20–30 m wide) canyon, ~150 m deep and 0.5 km long (Stokes et al., 2008). On exiting the canyon, the river turns to flow SW initially through a moderately open asymmetric valley, although the channel is entrenched in a bedrock channel (Fig. 10B) and then through the main Dades Gorge (Fig. 5G). The gorge cuts through structurally thickened Lower Jurassic limestone by >200 m for ~5 km (Stokes et al., 2008, 2017) and is <10 m in width in the upper part of the gorge.

All four DEMs show the gorges with increasing effective resolution from the ASTER through the SRTM30 and AW3D30 to the TanDEM-X DEM, although the ASTER data does not clearly show all three of the significant dip slope tributaries that flow into the Dades along this stretch of river. The TanDEM-X DEM does have higher average slopes and areas of roughness, this is in part to the result of the bedrock topography along the eastern margin of the gorge. It is also partly owing to previously mentioned coherence errors.

The constrained nature of the river course in this region results in a fairly good representative river network developed from all the DEMs (Figs. 7 and 9). Overall, the derived stream network from AW3D30 DEM is marginally the best for the main Dades Gorge and is somewhat more detailed than the other stream networks. Notably, all the networks sit to the east of the river on the adjacent hillslope along the broader valley between the two gorges.

Finally, area D is where the Dades River starts to traverse the main thrust front region forming the southern margin of the High Atlas Mountains (Fig. 11). As a result there are marked changes in the direction of the river as it passes through this region as it flows along the strike of the bedrock geology and the major tectonic structure, forming relatively open valleys along strike and short transverse reaches where gorges are developed (Stokes et al., 2017).

In this region, part of the ASTER GDEM is from the adjacent tile, and the effective resolution of that section of the DEM is much higher and comparable to the SRTM30 DEM. The AW3D30 is again superior to the other 30-m data sets but none matches the detail of the 12-m TanDEM-X data.

Of interest here is where the Dades River flows into a narrow gorge (Fig. 5H), three of the DEM-derived stream networks do not follow the true course of the river and cut to the north across a topographic saddle (Fig. 7D). By contrast, the AW3D30-derived network is the only one that follows the true course of the river through the narrow gorge. In general, upstream of this section the river network is unclear and none of the derived stream networks does a good job of representing the real river network. Downstream of the gorge improves, with DEMs producing a reasonable stream network configuration, although the ASTER data is noticeably the least representative.

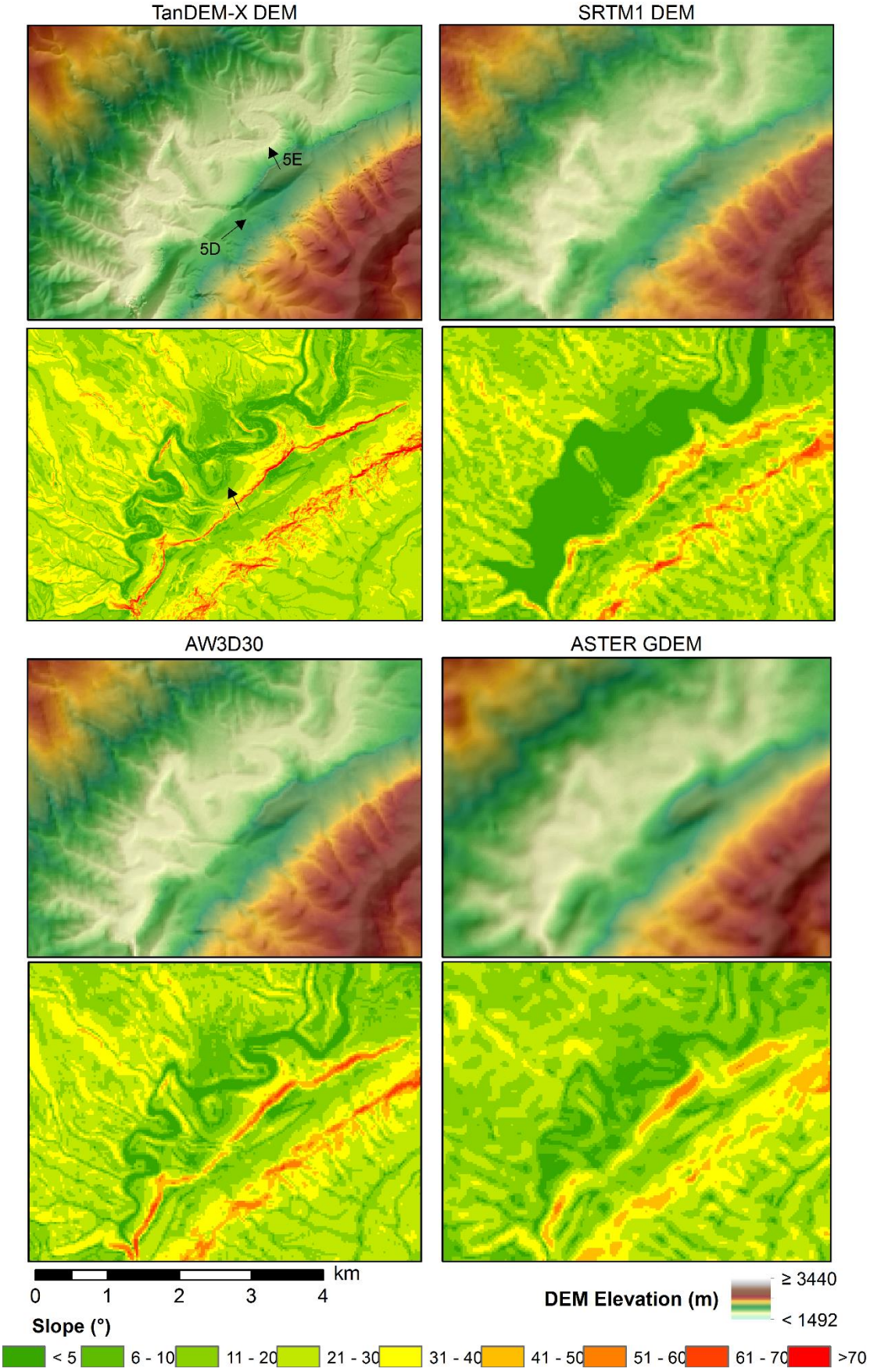

Fig. 8. DEM with underlying hillshade and slope raster for subarea B showing the difference between the four DEMs studied. The location and direction of photographs 5D-E are indicated.

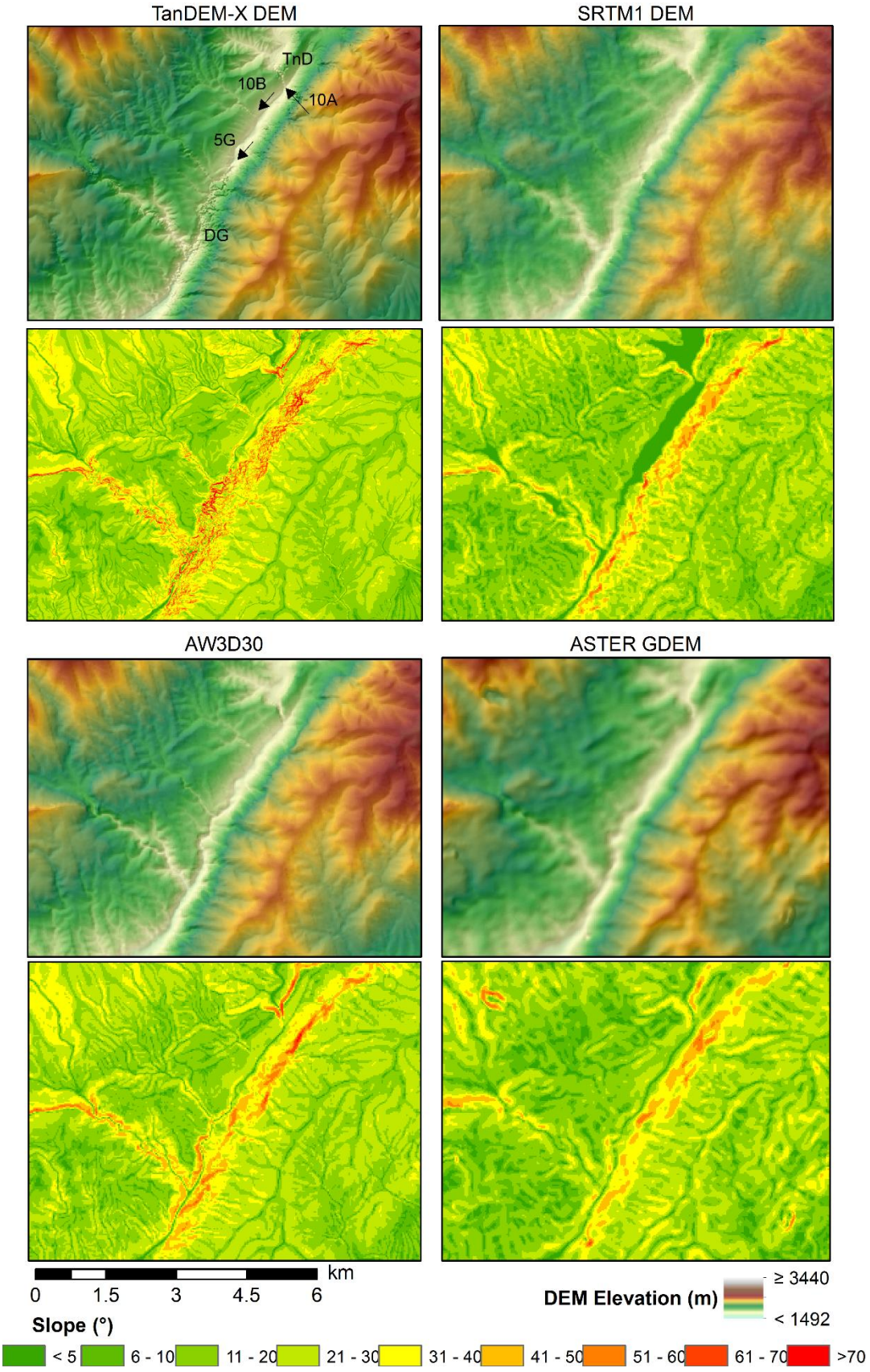

Fig. 9. DEM with underlying hillshade and slope raster for subarea C showing the difference between the four DEMs studied. The location and direction of photographs 5G, 10A, and 10B are indicated.

Fig. 10. (A) The Tarhía n'Dades Gorge looking upstream and (B) looking downstream from the Tarhía n'Dades Gorge, note the entrenched nature of the river in the bedrock channel.

In summary, the ASTER GDEM has the lowest effective resolution and produces the least accurate stream network. The SRTM data has a higher effective resolution but the DEM is still fairly smooth, but in most areas the stream network produced is representative of the river system. The average slopes and elevations of the GDEM and SRTM30 DEMs are fairly similar for the different areas considered. The AW3D30 data, although possessing the same grid spacing as the ASTER and SRTM30 data, has higher effective resolution producing the most accurate river network. By contrast, the TanDEM-X has the best level of detail and owing to the cell size, a more complex stream network that is fairly representative but suffers from channel routing errors in areas of high relief.

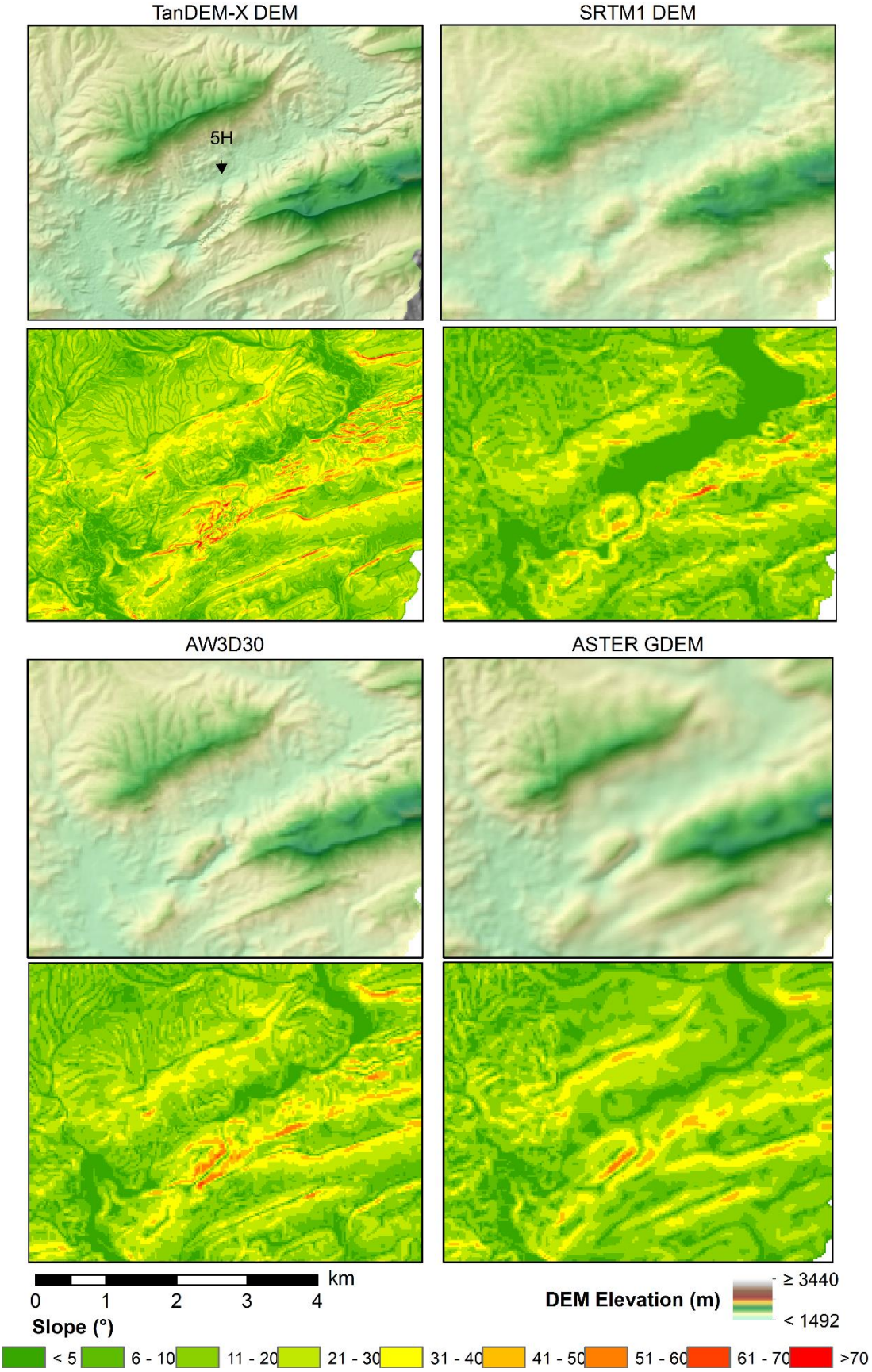

Fig. 11. DEM with underlying hillshade and slope raster for subarea D showing the difference between the four DEMs studied. The direction of photograph 5H is indicated.

6.2. DEM elevation vs. GPS measurements

The elevation of 77 points, mainly located along the main Dades River have been extracted from the four DEMs and compared to GPS measurements of elevation (supplemental data). Although caution is always wise when using GPS altimetry data, the values from the two sources show a strong correlation (Fig. 12), with an $R^2 > 0.9$ for all four DEMs. All data sets show strong positive correlations, with the TanDEM-X DEM data being marginally closer to the GPS data indicated by the higher R^2 value and lowest *y*-axis intercept of 4.4 m.

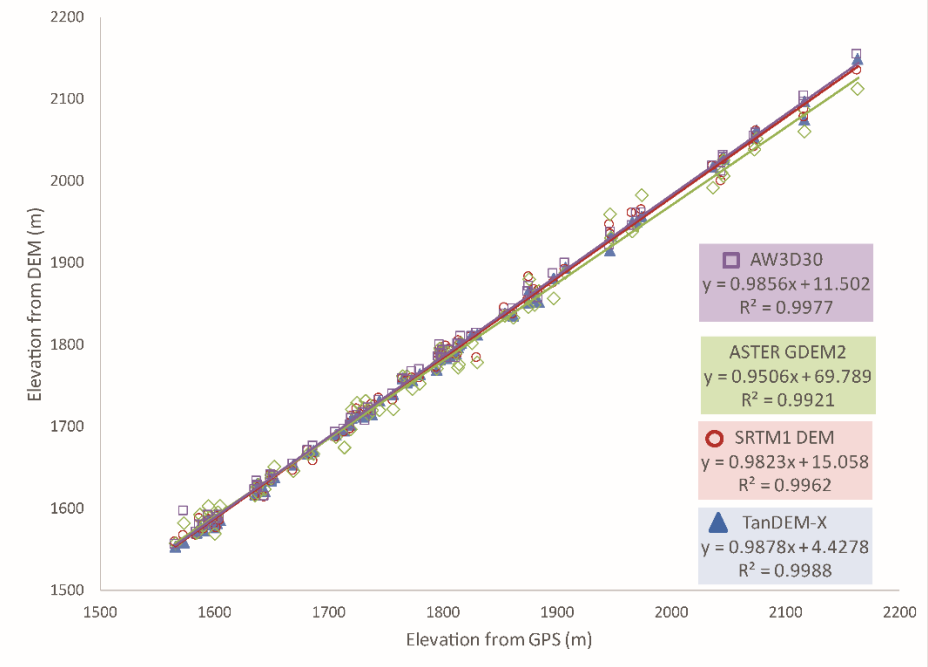

Fig. 12. Elevation as extracted from the four DEM data sets against field measured elevation from a handheld GPS.

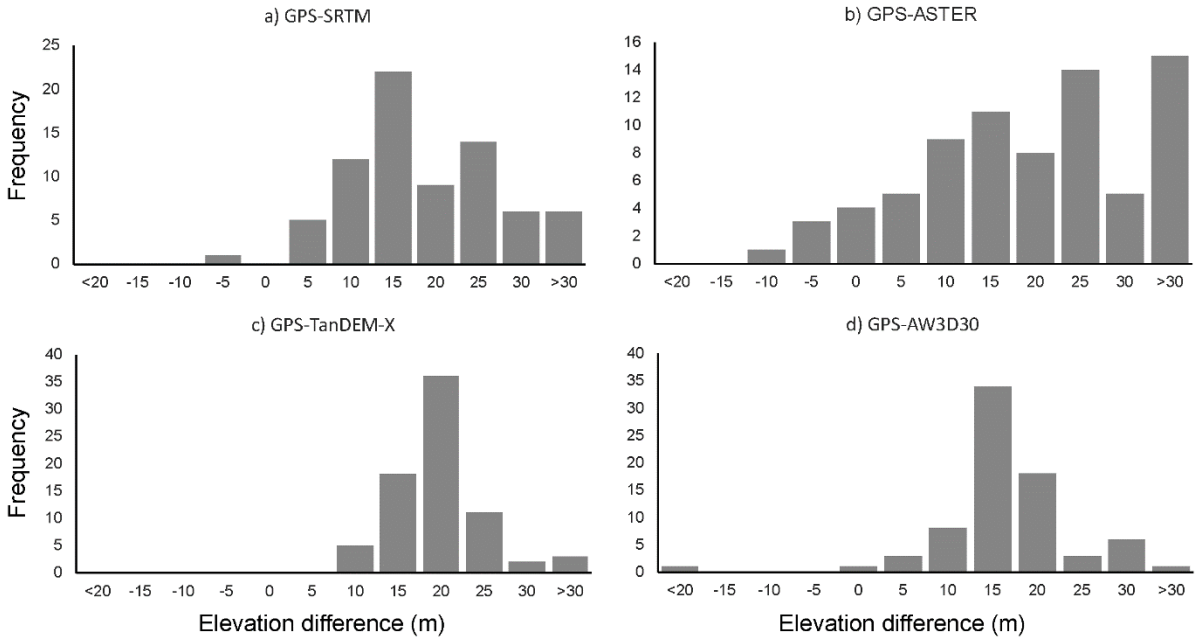

Fig. 13. Histograms of elevation differences between GPS measurements and DEM cell values for the same location.

The relative frequency distribution of the difference in elevation between GPS measurements and values extracted from the four DEMs (Fig. 13) shows a stark difference between the ASTER data and the other DEMs. The ASTER data shows a marked difference between the GPS and DEM data, when compared to other DEMs. There are 15 locations where the difference between the ASTER DEM and GPS elevation is >30 m, and more locations where the ASTER DEM returns higher elevations than the GPS than for the other DEMS. In general, the ASTER DEM to GPS comparison shows a wider spread in values than for the other DEMs investigated. All data sets have positive skews as a result of the DEMs having generally lower values than the GPS measurements. While the difference between the TanDEM-X and AW3D30 DEMs is the least variable, the DEM returns values 15–20 m lower than the GPS readings.

6.3. Slope-area plots

River long profiles were extracted for the Dades River from each of the data sets (Fig. 14A) using the same initial coordinates and coverage. Overall, each DEM produces a subtly different profile and a different slope-area *SA* plot. The long profile determined from the ASTER DEM is the shortest with a river length of ~180 km (Table 2). The SRTM30 and AW3D30 derived profiles have a similar shape overall to the ASTER river profile and the height of the headwaters is practically the same, although the AW3D30 profile is slightly shorter (by 2 km) than the SRTM river long profile. The SRTM30 profile is slightly noisier in the main knickpoints compared to the ASTER data, whereas the AW3D30 has little noise and virtually no smoothing has been required of the raw DEM to produce the final river long profile. The river long-profile from the TanDEM-X data is the longest at 207 km. The TanDEM-X river profile is the most smoothed compared to the raw DEM data.

For all DEMs, four main river sections can be identified on the *SA* plots (Figs. 14B-D). The most upstream section of the river (reach 1; Table 2) is the most variable in terms of the shape of the river long profile and in the values derived from the *SA* plot. The TanDEM-X data gives the lowest k_{sn} value at 8.4 $m^{0.9}$ and the lowest concavity (0.27); whereas the AW3D30, ASTER, and SRTM30 data are more similar with moderate concavity (Θ = 0.57 – 0.61) and similar k_{sn} values of 17.1 to 18.7 $m^{0.9}$ (Table 2).

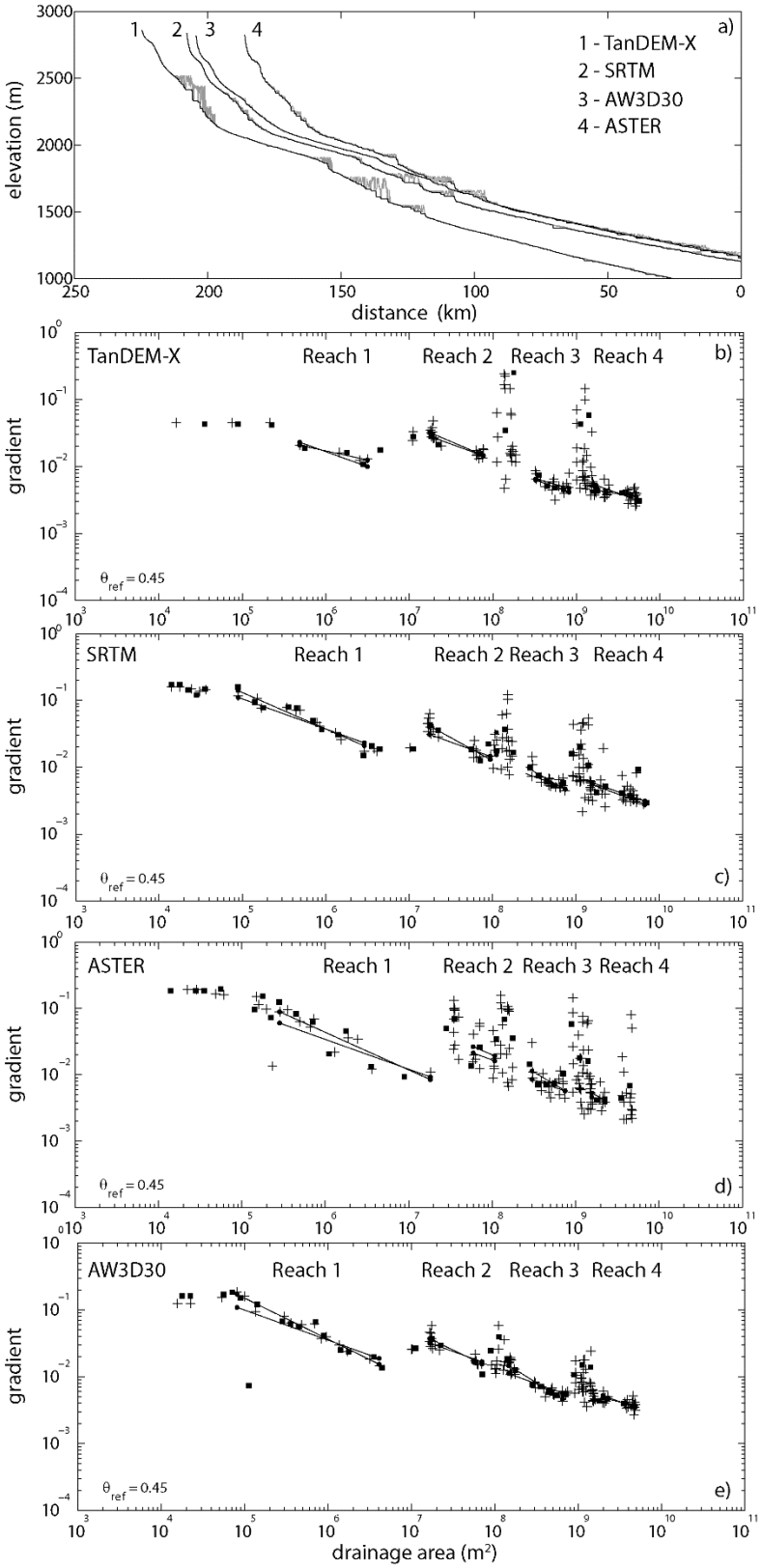

Fig. 14. (A) River long profile of the Dades River extracted from the TanDEM-X, SRTM30, ASTER GDEM2, and AW3D30 data sets; the black line shows the smoothed profile, whereas the grey line shows the raw DEM data. Note the TanDEM-X profile has been shifted 25 m on the X axis to enhance the clarity of the figure. (B – E) Slope-area plots for the Dades River from each of the DEMs using 0.45 as the reference concavity.

Table 2 Normalised steepness index K_{sn} and concavity Θ calculated for the four identified reaches of the Dades River from the four DEMs studied and for the 90-m SRTM data (SRTM90) as used by Boulton et al. (2014) for the same study area

Data set	Total		Reach 1 (highest)			Reach 2			Reach 3			Reach 4 (lowest)		
	Area (km^2)	Length (km)	K_{sn}	Θ	±	K_{sn}	Θ	±	K_{sn}	Θ	±	K_{sn}	Θ	±
TanDEM-X	1620.0	207	8.4	0.27	0.19	51.2	0.63	0.16	42.5	0.34	0.4	75.5	0.2	0.21
SRTM30	1622.5	203	18.7	0.57	0.12	56.4	0.69	0.21	48.9	0.72	0.36	80.8	0.44	0.44
ASTER	1627.1	181	17.1	0.57	0.21	66.9	0.53	1.8	56.1	0.75	0.7	63	0.67	2.2
AW3D30	1620.7	201	17.7	0.61	0.07	56.8	0.61	0.19	52.7	0.77	0.13	79.9	0.29	0.19
SRTM90	1614.5	140	11.3	0.25	0.72	47.6	0.87	1.5	50.6	0.76	0.56	71.6	0.18	0.69

All profiles then exhibit a clear slope-break knickpoint and a two-three fold increase in the k_{sn} downstream of the knickpoint (0.53 to 0.69 $m^{0.9}$) forming reach 2. Concavity is similar for the TanDEM-X, SRTM30, and AW3D30 data (0.16–0.21), yet significantly higher for the ASTER data where $\Theta = 1.8$. Reach 3 is separated from reach 2 by a vertical step knickpoint with a small drop in the k_{sn} across all of the data sets ($k_{sn} = 42.5$ to 56.1 $m^{0.9}$). The concavity determined from the TanDEM-X is lower ($\Theta = 0.34$) compared to the river profiles determined from the other DEMs, where a concavity of 0.72–0.77 is returned.

The lowest reach (section 4) runs from the junction of the river in the Ouarzazate basin to the top of the incised reach at M'smirir taking in the main Dades Gorge, the Tarhía n'Dades Gorge, and the bedrock meanders and is the main knickzone identified by Boulton et al. (2014). The shape of the *SA* plot indicates a mixed vertical step and slope-break form. The calculated normalised steepness index k_{sn} varies from 80.8 $m^{0.9}$ from the SRTM data to 63 $m^{0.9}$ from the ASTER data (Fig. 14, Table 2). The AW3D30 data gives a k_{sn} of 79.9 $m^{0.9}$ and the TanDEM-X data gives a value sitting at 75.5 $m^{0.9}$, therefore all showing an increase in k_{sn} from reach 3 of 1.2 (ASTER) to 1.6 times. Measured concavity is, by contrast, much more variable despite overall similarity in the profiles (Table 2).

7. Discussion

7.1. Limitations and strengths of data sets

The different DEMs assessed have individual strengths and weaknesses for the High Atlas mountain landscape region as revealed by the above analyses. The ASTER data clearly have the lowest effective resolution as previously reported in other studies (Rexer and Hirt, 2014; Baade and Schmullius, 2016). Furthermore, in this study area the data are also affected with a previously undescribed issue, as there is no appreciable difference in resolution between the older GDEM1 and newer GDEM2 releases. In addition, the ASTER data have the highest number of pits of any of the studied DEMs and weakest correlations to the GPS data (Fig. 13). Some authors have reported that ASTER is better than SRTM90 data for river profile analysis for certain areas (e.g., Kent et al., 2017), but the release of the global SRTM30 dataset clearly supersedes the ASTER data for most areas rendering this DEM unsuitable for

many applications (Purinton and Bookhagen, 2017). That is not to say that the SRTM30 data is error free, it has the second worst fit with the GPS data, and the High Atlas region is affected by a missing sliver between tiles; no doubt other areas may suffer similar coverage issues.

The newer AW3D30 and TanDEM-X DEMs have much higher effective spatial resolutions than the ASTER and SRTM30 DEMs, whereby analysis of accompanying quality control data indicates that only small areas of the study area are affected by data quality issues. The AW3D30 data in particular has almost no issues for the Dades catchment, this is likely to the result of the highest number of coverages for the areas coinciding with the highest relief areas of the landscape (Appendix Fig. B). It is also possible that much precision has been retained in the 30-m product as a result of down sampling from the 5-m DEM. Although the quality is excellent in this study area, similar findings have not been documented by other recent studies. Hu et al. (2016) hypothesized that resampling of the 5-m product had considerable negative effect on the quality of the DEM for their study area in China, which they found to be similar in quality to the SRTM30 dataset, while Purinton and Bookhagen (2017) found DEM artefacts leading to issues with landscape representation. However, both of these studies used the 2016 version of the AW3D30 DEM that was of lower quality than the 2017 release.

By contrast, the TanDEM-X data shows decorrelation problems in areas of high relief, especially along the sides of gorges or along steep cliff lines, resulting in noise and higher slope values than derived from the other data sets (e.g., Fig. 4; Table 1). Higher slope values for the TanDEM-X compared to other DEMs was also recorded by Purinton and Bookhagen (2017), which they partly explained as the result of better resolution of rocky outcrops in other very steep areas. This may also be the case here but the consistency data clearly shows that there are data problems in these high relief areas resulting in height errors of up to 21 m, despite stack numbers of at least five coverages (Appendix Figure A). Yet the overall height accuracy of the TanDEM-X DEM has been shown to be excellent, with ~10 m global height accuracy at 90% linear error and with the majority of Africa having an absolute height accuracy of 2–5 m (Wecklich et al., 2015).

These errors no doubt combine to affect the results of the channel network extraction. The ASTER and TanDEM-X DEMs that have identified issues with resolution and decorrelation produce the least accurate flow networks (Fig. 7), demonstrating that increasing DEM resolution will not necessarily result in more accurate results from the D8 algorithm (Ariza-Villaverde et al., 2015). In areas of high relief, DEM resolution is clearly the limiting factor in developing a hydrologically sound network, as the scale of the topographic relief is below the resolution of the sensor. All of the DEMs studied here performed better than previous research undertaken using the SRTM90 data (Boulton et al., 2014) in areas such as the Dades Gorge. Yet the river networks in some of the more open valleys are also not well modelled by the D8 algorithm. The D8 algorithm is well known to perform poorly in areas of very low relief because flow can only be defined in eight possible directions (Turcotte et al., 2001). Furthermore, the higher vegetation density along the river valley floor (Fig. 5E and H) compared to the almost barren hillsides may cause reduced DEM accuracy (Sun et al., 2003; Hu et al., 2015), owing to the fact that the DEM acquisition methodology generally produces a canopy top model. However, SRTM DEMs are known to partly penetrate the vegetation canopy (Sun et al., 2003) perhaps suggesting why this dataset performs

better than the ASTER data. By contrast, the AW3D30 data derived from orthorectified imagery produces the most accurate stream network even in areas of high relief bedrock river meanders or narrow canyons. This accuracy may be owing to the 2.5-m accuracy of the original imagery.

The AWD30 DEM is also significantly more detailed than the SRTM30 and ASTER DEMs despite having the same 30-m grid size. This is especially noticeable in areas A, B, and D where the SRTM30 and ASTER DEMS produce fairly smoothed landscapes with little fine detail of the hillslopes and river valley resolvable. In these regions the resolution of the AW3D30 DEM is almost as good as the higher resolution TanDEM-X data, although neither data sets can resolve features such as the small river terraces described by Stokes et al. (2017). For the main Dades Gorge (area C), the AW3D30 data is a clearer product than the TanDEM-X owing to the high slope values in the higher resolution DEM obscuring some of the geomorphology, including the main river channel.

7.2. Implications for river long profile analysis

The analysis of slope-area plots to determine concavity and steepness index remain a widely used and powerful method for investigating river networks even with the advent of other methods to extract similar indices, such as the chi plots developed by Perron and Royden (2012), owing to the simplicity of the software and processing workflow. While attempts to improve and refine the extraction of the topographic indices have been carried out, only a few studies have investigated the impact of the choice of DEM or DEM grid size on the resultant parameters (i.e., Walker and Willgoose, 1999; Hancock et al., 2006; Wobus et al., 2006).

Interestingly, Finlayson and Montgomery (2003) found that there was a 51% decrease in k_s between 30 and 900 m data and a 30% increase in Θ. This is not the case with the Dades River where there is minimal variation in slope between the 12 and 30 m data for most river segments. There is a 47% decrease in k_{sn} observed in reach 1 between the 30 and 12 m data sets, but similar differences are not seen across the rest of the river profile data. The change in resolution studied here has a much smaller difference in resolution than that studied by Finlayson and Montgomery (2003), but even the SRTM90 data reported by Boulton et al. (2014) returned similar concavity and steepness indices for each of the river reaches (Table 2) to the higher resolution data sets. Therefore, our results support those of Wobus et al. (2006) and, more recently, Purinton and Bookhagen (2017) who found little variation in these topographic indices between different resolution data sets. Although our data do show more than the 10% variance reported by Wobus et al. (2006), likely the result of variable scatter of data on the *SA* plots (Fig. 13) . The SRTM30 and AW3D30 data have less noise and correspondingly fewer sinks needed to be filled in the DEM to form a hydrologically sound network. This results in lower errors on the concavity and overall similar values for both indices. By contrast, the ASTER and TanDEM-X data have much more scatter, likely the result of the poorer fit of the interpolated river network to the real river course. The highest errors are found associated with the SRTM90 data (Boulton et al., 2014), but the derived values of concavity and normalised steepness index are still in line with the higher resolution DEMs. However, the SRTM90 data obscures knickpoints in the most upstream reaches of the Dades catchment as a result of the lower resolution of this product.

Unlike Finlayson and Montgomery (2003), we also find no systematic increase in drainage area with increasing grid size but do note that the length of the river does decrease with grid size, with a 33% decrease in the length of the Dades River between the 12 and 90 m data. This is greater than the 17% loss in length reported by Finlayson and Montgomery (2003) or the 20% decrease in length documented by Fisher et al. (2013) for much greater changes in grid size. River length also seems susceptible to effective resolution as the ASTER data derives a river only ~90% of the length of that calculated from the SRTM30 and AW3D30 DEMs. As the effectiveness of the D8 algorithm ultimately controls the length of the modelled river, clearly grid size and accuracy are key parameters to the accurate modelling of the river (Ariza-Villaverde et al., 2015) but that finer grid sizes do not necessarily produce more accurate results. In summary, Θ and k_{sn} are consistent between the 30 and 12 m data sets indicating that the choice of DEM should not affect the overall interpretations regarding tectonic signals. But the error on the geomorphic indices or length of river will be affected by DEM choice and that the extracted river system should be cross-checked against topographic maps and/or satellite imagery to ensure accuracy and final choice of global DEM. Therefore, even with more accurate and higher resolution products it is still beholden on the geomorphologist to assess the usefulness of data sets for their individual study areas.

8. Conclusions

Here we have investigated the accuracy of four medium resolution global digital elevation models for use in fluvial geomorphic analysis and river long profile extraction. Two of the DEMs are widely used data sets (SRTM30 and ASTER), while the other two have recently become available to the scientific community and wider public (TanDEM-X and AW3D30). Our analyses have focussed upon commonly used and easily implemented tools within the GIS that are frequently used by geomorphologists, who may not be experts in remote sensing or advanced GIS computing, to determine the advantages and disadvantages of commonly utilised DEMs. Each DEM has different properties that would have implications for generic landscape analysis, but surprisingly the choice of DEM has little effect on the river long profile and derivative geomorphic indices.

Although the SRTM dataset was acquired the earliest, this DEM is still highly relevant. The SRTM30 does have a lower effective resolution than the TanDEM-X or AW3D30 DEM, but the river networks created from the SRTM30 DEM are more accurate than the newer and higher resolution TanDEM-X data, in line with the river profile data from the AW3D30 DEM.

In contrast, caution should be used with ASTER data; and as with previous studies a range of issues have been identified with the quality and accuracy of DEM. Largely this data set is superseded by the SRTM30 and newer AW3D30 DEMs, certainly for this area but probably for many other regions now that the SRTM30 data are available at a global scale.

The highest resolution DEM, the TanDEM-X has highest effective resolution and the level of map view topographic detail resolvable is impressive, but issues with data quality result in less accurate river networks in areas of high relief. In addition, unlike the other DEMs it is not free, but it is available at low cost (~100 Euros per tile) to the scientific community.

The newest DEM available, AW3D30, generates the best derivative river networksand is highly accurate even in areas of steep topography and high relief. The effective resolution is also surprisingly good and far better than the SRTM or ASTER DEMs. This new DEM shows great promise for future surface analyses across a range of disciplines.

Acknowledgements

This work would not have been possible without the generosity of government agencies sharing their data. The ALOS Global DSM is provided by and the copyright of JAXA. The SRTM data is provided by NASA and the USGS, and ASTER GDEM is a product of NASA and METI. The SRTM and ASTER data were retrieved from the EarthExplorer website courtesy of the NASA EOSDIS Land Processes Distributed Active Archive Center (LP DAAC), USGS/Earth Resources Observation and Science (EROS) Center, Sioux Falls, South Dakota. TanDEM-X data is the copyright of the German Aerospace Center (DLR). We also acknowledge funding in kind from DLR in the form of the TanDEM-X data. We also thank the editor, Richard Marston, and three anonymous reviewers for their support and comments that have improved this work.

References

Antón, L., De Vicente, G., Muñoz-Martín, A., Stokes, M., 2014. Using river long profiles and geomorphic indices to evaluate the geomorphological signature of continental scale drainage capture, Duero basin (NW Iberia). Geomorphology 206, 250-261.

Arboleya, M.-L., Babault, J., Owen, L.A., Teixell, A., Finkel, R.C., 2008. Timing and nature of Quaternary fluvial incision in the Ouarzazate foreland basin, Morocco. Journal of the Geological Society 165, 1059-1073.

Ariza-Villaverde, A.B., Jiménez-Hornero, F.J., de Ravé, E.G., 2015. Influence of DEM resolution on drainage network extraction: A multifractal analysis. Geomorphology 241, 243-254.

Aster GDEM Validation Team, 2009. ASTER Global DEM Validation.

Baade, J., Schmullius, C., 2016. TanDEM-X IDEM precision and accuracy assessment based on a large assembly of differential GNSS measurements in Kruger National Park, South Africa. ISPRS Journal of Photogrammetry and Remote Sensing 119, 496-508.

Babault, J., Van Den Driessche, J., Teixell, A., 2012. Longitudinal to transverse drainage network evolution in the High Atlas (Morocco): The role of tectonics. Tectonics 31, TC4020.

Bishop, M., Schroeder, J.F., 2004. Geographic information science and mountain geomorphology. Springer Science & Business Media. 486 pp.

Boulton, S.J., Whittaker, A.C., 2009. Quantifying the slip-rates, spatial distribution and evolution of active normal faults from geomorphic analysis: Field examples from an oblique-extensional graben, Southern Turkey. Geomorphology 104, 299-316.

Boulton, S.J., Stokes, M., Mather, A.E., 2014. Transient fluvial incision as an indicator of active faulting and Plio-Quaternary uplift of the Moroccan High Atlas. Tectonophysics 633, 16-33.

Chen, Y.C., Sung, Q., Cheng, K.Y., 2003. Along-strike variations of morphotectonic features in the Western Foothills of Taiwan: Tectonic implications based on stream-gradient and hypsometric analysis. Geomorphology 56, 109–137.

Das, S., Patel, P.P., Sengupta, S., 2016. Evaluation of different digital elevation models for analyzing drainage morphometric parameters in a mountainous terrain: a case study of the Supin--Upper Tons Basin, Indian Himalayas. SpringerPlus 5, 1544. doi.org/10.1186/s40064-016-3207-0.

Davis, W.M., 1903. The mountain ranges of the Great Basin. Bulletin Museum of Comparative Zoology XLII, 129-177

DiBiase, R.A., Heimsath, A.M., Whipple, K.X., 2012. Hillslope response to tectonic forcing in threshold landscapes. Earth Surface Processes and Landforms 37(8), 855-865.

DLR, 2016. TanDEM-X Ground Segment DEM Products Specification Document. TD-GS-PS-0021 v.3.1. DLR 46 pp.

Dłużewski, M., Krzemień, K., Rojan, E., Biejat, K., 2013. Stream channel development in the southern parts of the High Atlas Mountains, Morocco. Geografija 49, 10–21.

Farr, T.G., Rosen, P.A., Caro, E., Crippen, R., Duren, R., Hensley, S., Kobrick, M., Paller, M., Rodriguez, E., Roth, L., Seal, D., 2007. The shuttle radar topography mission. Reviews of Geophysics 45(2), RG2004, doi:10.1029/2005RG000183.

Finlayson, D.P., Montgomery, D.R., 2003. Modeling large-scale fluvial erosion in geographic information systems. Geomorphology 53(1),147-164.

Fisher, G.B., Bookhagen, B., Amos, C.B., 2013. Channel planform geometry and slopes from freely available high-spatial resolution imagery and DEM fusion: Implications for channel width scalings, erosion proxies, and fluvial signatures in tectonically active landscapes. Geomorphology 194, 46-56.

Fonstad, M.A., Dietrich, J.T., Courville, B.C., Carbonneau, P.E., 2013. Topographic structure from motion: a new development in photogrammetric measurements. Earth Surface Processes and Landforms 20, 817-827.

Frey, H., Paul, F., 2012. On the suitability of the SRTM DEM and ASTER GDEM for the compilation of: Topographic parameters in glacier inventories. International Journal of Applied Earth Observation and Geoinformation 18, 480–490.

Geudtner, D., 1995. Interferometric processing of ERS-1 SAR data. Cologne, Germany: Deutsche Forschungsanstalt fuer Luft- und Raumfahrt (DLR Forschungsbericht 95-28).

Gilbert, G.K., 1877 Report on the Geology of the Henry Mountains. US Government Printing Office.

Hancock, G.R., Martinez, C., Evans, K.G., Moliere, D.R., 2006. A comparison of SRTM and high-resolution digital elevation models and their use in catchment geomorphology and hydrology: Australian examples. Earth Surface Processes and Landforms 31, 1394-1412.

Haviv, I., Enzel, Y., Whipple, K.X., Zilberman, E., Matmon, A., Stone, J., Fifield, K.L., 2010. Evolution of vertical knickpoints (waterfalls) with resistant caprock: Insights from numerical modeling. Journal of Geophysical Research: Earth Surface 115(F3).

Hirano, A., Welch, R., Lang, H., 2003. Mapping from ASTER stereo image data: DEM validation and accuracy assessment. ISPRS Journal of Photogrammetry and Remote Sensing 57, 356-370.

Hirt, C., Filmer, M.S., Featherstone, W.E., 2010. Comparison and validation of the recent freely available ASTER-GDEM ver1, SRTM ver4.1 and GEODATA DEM-9S ver3 digital elevation models over Australia. Australian Journal of Earth Sciences 5, 337–347.

Hu, Z., Peng, J., Hou, Y., Shan, J., 2017. Evaluation of Recently Released Open Global Digital Elevation Models of Hubei, China. Remote Sensing 9, 262.

Jarvis, A., Reuter, H.I., Nelson, A., Guevara, E., 2008. Hole-filled SRTM for the globe Version 4, available from the CGIAR-CSI SRTM 90m Database (http://srtm.csi.cgiar.org).

Kent, E., Boulton, S. J., Whittaker, A.C., Stewart, I.S., Alçiçek, M.C., 2017. Normal fault growth and linkage in the Gediz (Alaşehir) Graben, Western Turkey, revealed by transient river long-profiles and slope-break knickpoints. Earth Surface Process and Landforms 42, 836-852.

Kirby, E., 2003. Distribution of active rock uplift along the eastern margin of the Tibetan Plateau: Inferences from bedrock channel longitudinal profiles. Journal of Geophysical Research, 108(B4).

Kirby, E., Whipple, K.X., 2012. Expression of active tectonics in erosional landscapes. Journal of Structural Geology 44, 54-75.

Martins, A.A., Cabral, J., Cunha, P.P., Stokes, M., Borges, J., Caldeira, B., Martins, A.C., 2017. Tectonic and lithological controls on fluvial landscape development in central-eastern Portugal: Insights from long profile tributary stream analyses. Geomorphology 276, 144-163.

Massong, T.M., Montgomery, D.R., 2000. Influence of sediment supply, lithology, and wood debris on the distribution of bedrock and alluvial channels. Geological Society of America Bulletin 112, 591-599.

Mather, A.E., Stokes, M., 2017. Bedrock structural control on catchment-scale connectivity and alluvial fan processes, High Atlas Mountains, Morocco. In: Ventra, D., Clarke, L.E., (Eds.) Geology and Geomorphology of Alluvial and Fluvial Fans: Terrestrial and Planetary Perspectives. Geological Society, London, Special Publications 440, SP440-15. doi: 10.1144/SP440.15

Mather, A.E., Stokes, M., Whitfield, E., 2017. River terraces and alluvial fans: the case for an integrated Quaternary fluvial archive. Quaternary Science Reviews, 166, 74-90.

McMaster, K.J., 2002. Effects of digital elevation model resolution on derived stream network positions. Water Resources Research 38 (4), doi: 10.1029/2000WR000150

Micheletti, N., Chandler, J.H., Lane, S.N., 2015. Structure from motion (SFM) photogrammetry. In: Clarke, L.E., Nield, J.M. (Eds.) Geomorphological Techniques (Online Edition). London: British Society for Geomorphology. ISSN: 2047-0371, https://dspace.lboro.ac.uk/dspace-jspui/bitstream/2134/17493/3/2.2.2_sfm.pdf [date accessed 01/03/2018].

Montgomery, D.R., Dietrich, W.E., Sullivan, K., 1998. The role of GIS in watershed analysis. In: Lane, S.N., Richards, K.S., Chandler J.H., (Eds) Landform monitoring, modelling, and analysis. John Wiley & Sons, Chichester, UK, pp. 241-261.

Moore, I.D., Grayson, R.B., Ladson, A.R., 1991. Digital terrain modelling: a review of hydrological, geomorphological, and biological applications. Hydrological processes 5(1), 3-30.

Mukherjee, S., Joshi, P.K., Mukherjee, S., Ghosh, A., Garg, R.D., Mukhopadhyay, A., 2013. Evaluation of vertical accuracy of open source Digital Elevation Model (DEM). International Journal of Applied Earth Observation and Geoinformation 21, 205-217.

NASA Land Processes Distributed Active Archive Center. 2001. ASTER L1B DEM. USGS/Earth Resources Observation and Science (EROS) Center, Sioux Falls, South Dakota.

O'Callaghan, J.F., Mark, D.M., 1984. The extraction of drainage networks from digital elevation data. Computer vision, graphics, and image processing 28, 323-344.

Pastor, A., Babault, J., Teixell, A., Arboleya, M.L., 2012. Intrinsic stream-capture control of stepped fan pediments in the High Atlas piedmont of Ouarzazate (Morocco). Geomorphology 173-174, 88-103.

Perron, J.T., Royden, L., 2013. An integral approach to bedrock river profile analysis. Earth Surface Processes and Landforms 38(6), 570-576.

Persendt, F. C., Gomez, C., 2016. Assessment of drainage network extractions in a low-relief area of the Cuvelai Basin (Namibia) from multiple sources: LiDAR, topographic maps, and digital aerial orthophotographs. Geomorphology 260, 32-50.

Petit, C., Goren, L., Rolland, Y., Bourlès, D., Braucher, R., Saillard, M., Cassol, D., 2017. Recent, climate-driven river incision rate fluctuations in the Mercantour crystalline massif, southern French Alps. Quaternary Science Reviews 165, 73-87.

Pipaud, I., Loibl, D., Lehmkuhl, F., 2015. Evaluation of TanDEM-X elevation data for geomorphological mapping and interpretation in high mountain environments — A case study from SE Tibet, China. Geomorphology 246, 232–254.

Purinton, B., Bookhagen, B., 2017. Validation of digital elevation models (DEMs) and comparison of geomorphic metrics on the southern Central Andean Plateau. Earth Surface Dynamics 5(2), 211 – 237.

Rabus, B., Eineder, M., Roth, A., Bamler, R., 2003. The shuttle radar topography mission- a new class of digital elevation models acquired by spaceborne radar. ISPRS journal of photogrammetry and remote sensing 57, 241-262.

Regalla, C., Kirby, E., Fisher, D., Bierman, P., 2013. Active forearc shortening in Tohoku, Japan: Constraints on fault geometry from erosion rates and fluvial longitudinal profiles. Geomorphology 195, 84–98.

Rexer, M., Hirt, C., 2014. Comparison of free high resolution digital elevation data sets (ASTER GDEM2, SRTM v2. 1/v4. 1) and validation against accurate heights from the Australian National Gravity Database. Australian Journal of Earth Sciences 61(2), 213-226.

Roda-Boluda, D.C., Whittaker, A.C., 2018. Normal fault evolution and coupled landscape response: examples from the Southern Apennines, Italy. Basin Research 30(S1), 186-209.

Rodriguez, E., Morris, C.S., Belz, J.E., Chapin, E.C., Martin, J.M., Daffer, W., Hensley, S., 2005. An assessment of the SRTM topographic products. Technical Report JPL D-31639, Jet Propulsion Laboratory, Pasadena, California, 143 pp.

Rodriguez, E., Morris, C.S., Belz, J.E., 2006. A global assessment of the SRTM performance. Photogrammetric Engineering & Remote Sensing 72, 249-260.

Roering, J.J., Mackey, B.H., Marshall, J.A., Sweeney, K.E., Deligne, N.I., Booth, A.M., Handwerger, A.L., Cerovski-Darriau, C., 2013. 'You are HERE': Connecting the dots with airborne lidar for geomorphic fieldwork. Geomorphology 200, 172-183.

Rossi, M.W., Quigley, M.C., Flectcher, J.M., Whipple, K.X., Diaz-Torres, J.J. Seiler, C., Fifield, L.K., Heimsath, A.M., 2017. Along-strike variation in catchment morphology and cosmogenic denudation rates reveal the pattern and history of footwall uplift, Main Gulf Escarpment, Baja California. Bulletin of the Geological Society of America 129(7–8), 837–854.

Schneevoigt, N.J., van der Linden, S., Thamm, H.P., Schrott, L., 2008. Detecting Alpine landforms from remotely sensed imagery. A pilot study in the Bavarian Alps. Geomorphology 93(1), 104-119.

Schneider, A., Jost, A., Coulon, C., Silvestre, M., Théry, S., Ducharne, A., 2017. Global-scale river network extraction based on high-resolution topography and constrained by lithology, climate, slope, and observed drainage density. Geophysical Research Letters 44 (6), 2773-2781.

Schulz, O., Busche, H., Benbouziane, A., 2008. Decadal precipitation variances and reservoir inflow in the semi-arid Upper Drâa basin (South-Eastern Morocco). In: Zereini, F., Hötzl, H. (Eds.), Climatic Change and Water Resources in the Middle East and North Africa. Springer, Heidelberg, pp. 165–178.

Sinclair, H.D., Mudd, S.M., Dingle, E., Hobley, D.E.J., Robinson, R., Walcott, R., 2017. Squeezing river catchments through tectonics: Shortening and erosion across the Indus Valley, NW Himalaya. Geological Society of America Bulletin 129(1-2), 203-217.

Smith, M.J., Pain, C.F., 2009. Applications of remote sensing in geomorphology. Progress in Physical Geography 33(4), 568-582.

Smith, B., Sandwell, D., 2003. Accuracy and resolution of shuttle radar topography mission data. Geophysical Research Letters 30(9).

Stäblein, G., 1988. Geomorphological aspects of the Quaternary evolution of the Ouarzazate Basin, Southern Morocco. Lecture Notes in Earth Sciences 15, 433–443.

Stokes, M., Mather, A.E., 2015. Controls on modern tributary-junction alluvial fan occurrence and morphology: High Atlas Mountains, Morocco. Geomorphology 248, 344-362.

Stokes, M., Mather, A.E., Belfoul, A., Farik, F., 2008. Active and passive tectonic controls for transverse drainage and river gorge development in a collisional mountain belt (Dades Gorges, High Atlas Mountains, Morocco). Geomorphology 102, 2–20.

Stokes, M., Mather, A.E., Belfoul, M., Faik, F., Bouzid, S., Geach, M.R., Cunha, P.P., Boulton, S.J., Thiel, C., 2017. Controls on dryland mountain landscape development along the NW Saharan desert margin: Insights from Quaternary river terrace sequences (Dadès River, south-central High Atlas, Morocco). Quaternary Science Reviews 166, 363-379.

Stübner, K., Grin, E., Hidy, A.J., Schaller, M., Gold, R.D., Ratschbacher, L.,Ehlers, T., 2017. Middle and Late Pleistocene glaciations in the southwestern Pamir and their effects on topography. Earth and Planetary Science Letters 466, 181-194.

Sun, G. Ranson, K. Kharuk, V. Kovacs, K. 2003. Validation of surface height from Shuttle Radar Topography Mission using shuttle laser altimeter. Remote Sensing of the Environment 4, 401–411.

Tachikawa, T., Kaku, M., Iwasaki, A., Gesch, D.B., Oimoen, M.J., Zhang, Z., Danielson, J.J., Krieger, T., Curtis, B., Haase, J., Abrams, M., 2011. ASTER global digital elevation model version 2-summary of validation results. NASA pp 27.

Tadono, T.,Ishida, H., Oda, F., Naito, S., Minakawa, K., Iwamoto, H., 2014. Precise Global DEM Generation by ALOS PRISM. ISPRS Annals of the Photogrammetry, Remote Sensing and Spatial Information Sciences II-4, 71-76.

Tadono, T., Nagai, H., Ishida, H., Oda, F., Naito, S., Minakawa, K., Iwamoto H., 2016. Initial Validation of the 30 m-mesh Global Digital Surface Model Generated by ALOS PRISM. The International Archives of the Photogrammetry, Remote Sensing and Spatial Information Sciences, ISPRS, XLI-B4, 157-162.

Tarboton, D.G., Bras, R.L., Rodriguez-Iturbe, I., 1991. On the extraction of channel networks from digital elevation data. Hydrological Processes 5 (1), 81-100

Toutin, T., 2002. Impact of terrain slope and aspect on radargrammetric DEM accuracy. ISPRS Journal of Photogrammetry and Remote Sensing 57(3), 228-240.

Turcotte, R., Fortin, J.P., Rousseau, A.N., Massicotte, S., Villeneuve, J.P., 2001. Determination of the drainage structure of a watershed using a digital elevation model and a digital river and lake network. Journal of Hydrology 240, 225-242.

Walker, J.P., Willgoose, G.R., 1999. On the effect of digital elevation model accuracy on hydrology and geomorphology. Water Resources Research 35, 2259– 2268.

Walsh, L.S., Martin, A.J., Ojha, T.P., Fedenczuk, T., 2012. Correlations of fluvial knickzones with landslide dams, lithologic contacts, and faults in the southwestern Annapurna Range, central Nepalese Himalaya. Journal of Geophysical Research: Earth Surface 117, 1–24.

Wecklich, C., Gonzalez, C., Bräutigam, B., Bachmann, M., 2015. Height accuracy for the first part of the global TanDEM-X DEM data. Geomorphometry for Geosciences, 5-8.

Werner, M., 2001. Shuttle Radar Topography Mission (SRTM), Mission overview. Frequenz 55, 75-79

Westoby, M.J., Brasington, J., Glasser, N.F., Hambrey, M.J., Reynolds, J.M., 2012. Structure-from-Motion' photogrammetry: A low-cost, effective tool for geoscience applications. Geomorphology 179, 300-314

Whipple, K.X., Tucker, G.E., 2002. Implications of sediment-flux-dependent river incision models for landscape evolution. Journal of Geophysical Research: Solid Earth 107(B2).

Whittaker, A.C., Boulton S.J., 2012. Tectonic and climatic controls on knickpoint retreat rates and landscape response times, Journal of Geophysical Research-Earth Surface 117: F02024. doi:10.1029/2011JF002157

Whittaker, A.C., Cowie, P.A., Attal, M., Tucker, G.E., Roberts, G.P., 2007. Contrasting transient and steady-state rivers crossing active normal faults: New field observations from the central Apennines, Italy. Basin Research 19, 529–556.

Wobus, C.W., Whipple, K.X., Kirby, E., Snyder, N., Johnson J., Spyropolou, K., Crosby, B., Sheehan, D., 2006. Tectonics from topography: procedures, promise,

pitfalls. In: Willett, S., Hovius, N., Brandon, M., Fisher, D., (Eds.), Tectonics, Climate and Landscape Evolution. AGU Special Paper 398, 55-74.

Yanites, B.J., Tucker, G.E., 2010. Controls and limits on bedrock channel geometry. Journal of Geophysical Research: Earth Surface 115(4).

Zhang, W., Montgomery, D.R., 1994. Digital elevation model grid size, landscape representation, and hydrologic simulations. Water Resources Research 30, 1019–1028.

Zhang, X., Drake, N.A., Wainwright, J., Mulligan, M., 1999. Comparison of slope estimates from low resolution DEMs: scaling issues and fractal method for their solution. Earth Surface Processes and Landforms 24, 763– 779.

Appendices

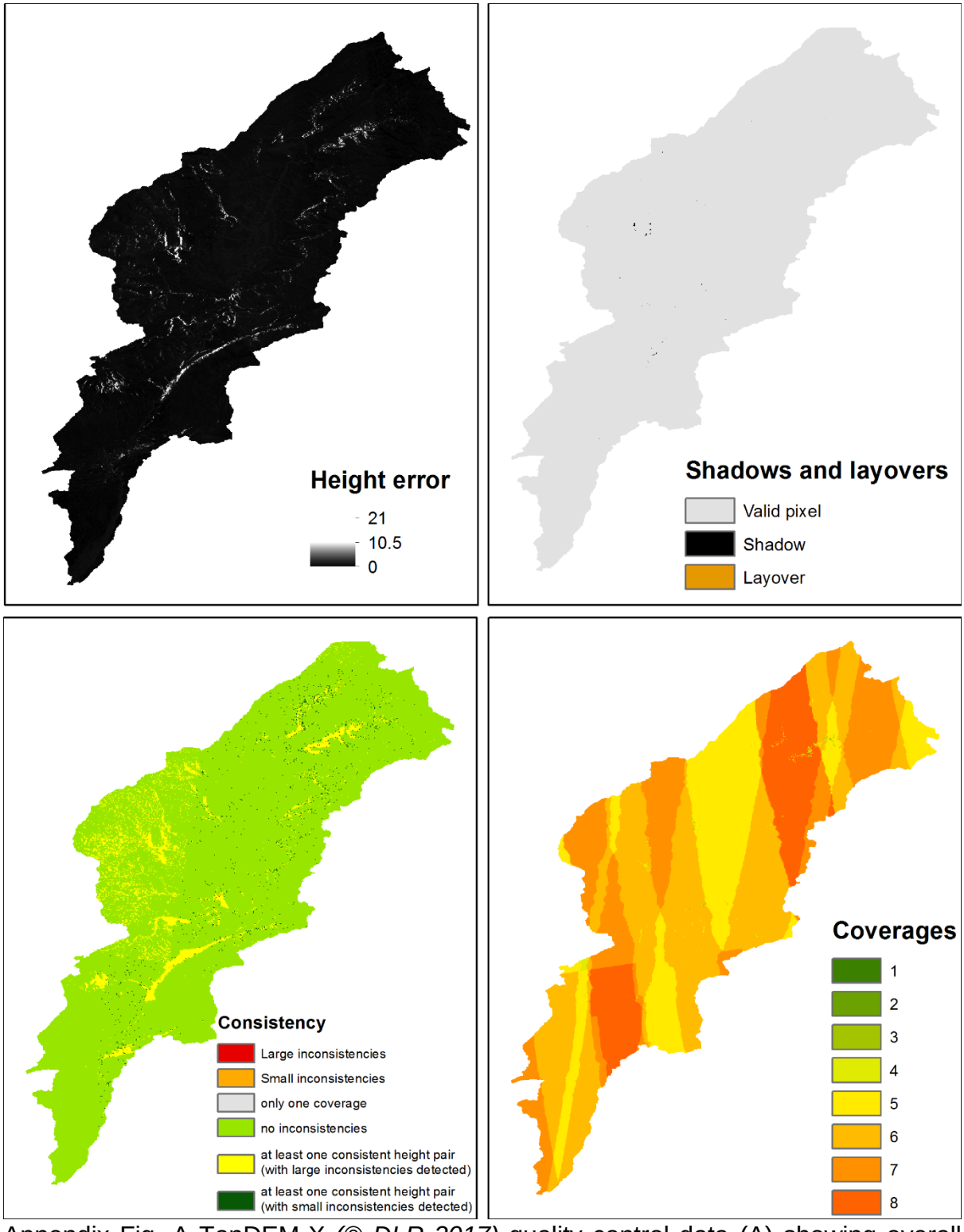

Appendix Fig. A TanDEM-X *(© DLR 2017)* quality control data (A) showing overall height error across the Dades catchment. (B) location of pixels identified as having shadows or layovers compared to valid pixels. (C) map showing any inconsistent height pairs in the catchment. (D) number of coverages used to make the DEM.

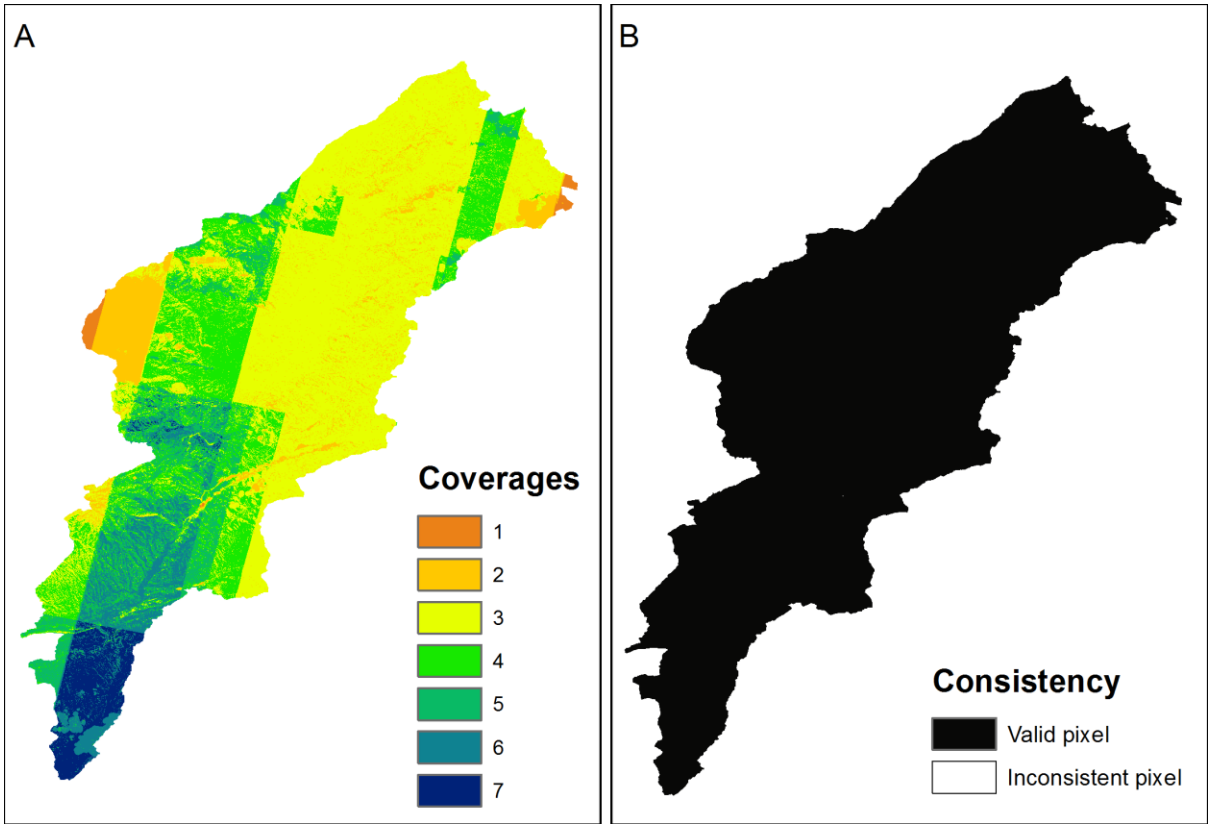

Appendix Fig. B. Quality control data for the Dades catchment for the AW3D30 *(© JAXA 2017)* data, (A) map showing the number of coverages used to make the DEM and (B) the validity of pixels across the area.

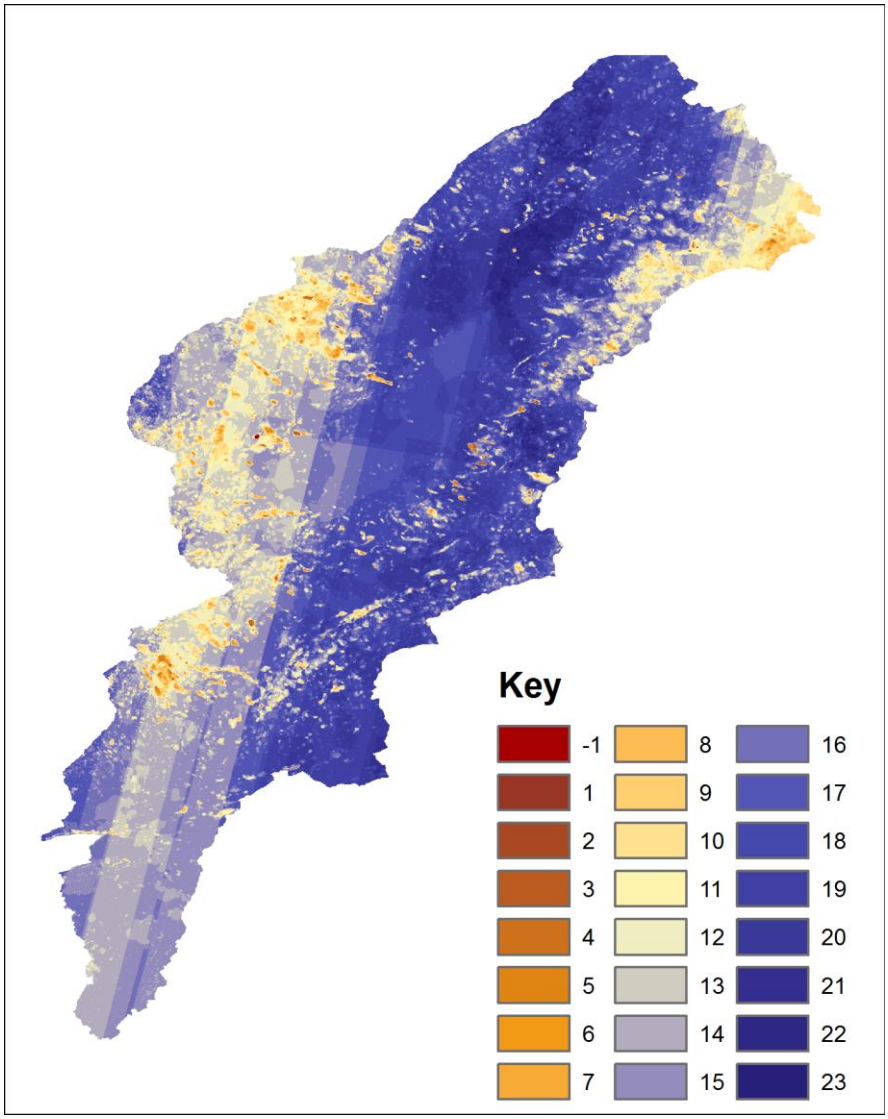

Appendix Fig. C. Map of the Dades catchment showing the number of coverages used to make the ASTER GDEM2 DEM, where -1 indicates pixels filled with SRTM90 data.